bioRxiv preprint doi: https://doi.org/10.1101/2020.07.30.228759; this version posted July 30, 2020. The copyright holder for this preprint (which was not certified by peer review) is the author/funder. All rights reserved. No reuse allowed without permission.

RIP140 inhibits glycolysis-dependent proliferation of cancer cells by regulating transcriptional crosstalk between hypoxia induced factor and p53

Valentin Jacquier, Delphine Gitenay[*], Samuel Fritsch, Laetitia K. Linares, Sandrine Bonnet, Stéphan Jalaguier, Vincent Cavaillès[#§] and Catherine Teyssier[#§]

IRCM, Institut de Recherche en Cancérologie de Montpellier, INSERM U1194, Université Montpellier, Montpellier F-34298, France

[*]present address: IRMB, University of Montpellier, INSERM, CNRS, CHU Montpellier, Montpellier, France

[#]Co-last authors

[§]Corresponding authors: catherine.teyssier@inserm.fr (C.T.); vincent.cavailles@inserm.fr (V.C.)

bioRxiv preprint doi: https://doi.org/10.1101/2020.07.30.228759; this version posted July 30, 2020. The copyright holder for this preprint (which was not certified by peer review) is the author/funder. All rights reserved. No reuse allowed without permission.

Abstract

Cancer cells with uncontrolled proliferation preferentially depend on glycolysis to grow, even in the presence of oxygen. Cancer cell proliferation is sustained by the production of glycolytic intermediates, which are diverted into the pentose phosphate pathway. The transcriptional co-regulator RIP140 represses the activity of transcription factors that drive cell proliferation and metabolism, especially glycolysis. However, it is still unknown whether RIP140 is involved in cancer-associated glycolysis deregulation, and whether this involvement could impact tumor cell proliferation. Here we use cell proliferation and metabolic assays to demonstrate that RIP140-deficiency causes a glycolysis-dependent increase in breast tumor growth. RIP140 inhibits the expression of the glucose transporter GLUT3 and of the Glucose-6-Phosphate Dehydrogenase G6PD, the first enzyme of the pentose phosphate pathway. RIP140 thus impacts both this pathway and glycolysis to block cell proliferation. We further demonstrate that RIP140 and p53 jointly inhibit the transcription of the GLUT3 promoter, induced by the hypoxia inducible factor HIF-2α. Overall, our data establish RIP140 as a critical modulator of the p53/HIF cross-talk that controls cancer glycolysis.

bioRxiv preprint doi: https://doi.org/10.1101/2020.07.30.228759; this version posted July 30, 2020. The copyright holder for this preprint (which was not certified by peer review) is the author/funder. All rights reserved. No reuse allowed without permission.

Keywords: cancer cell metabolism, transcription, RIP140, hypoxia, breast cancer, p53, glycolysis, GLUT3, pentose phosphate pathway, G6PD.

Introduction

In a normal resting cell, glycolysis converts glucose to pyruvate, which enters the tricarboxylic acid cycle where it becomes oxidized to generate ATP into mitochondria. In the absence of oxygen, glucose is still degraded into pyruvate, which is now converted into lactate in the cytosol. On switching to proliferative mode, cells increases glycolysis and reduce oxidative phosphorylation, which results in a high rate of glycolysis leading to lactate production. This metabolic switch was first described by Otto Warburg in the 20's, who observed that cancer cells prefer glycolysis to mitochondrial respiration to produce energy, even in the presence of oxygen (Hsu and Sabatini, 2008). This conversion of glucose to lactate in the presence of oxygen is now established as the Warburg effect, or aerobic glycolysis. At first, Warburg hypothesized that cancer arises from impaired mitochondria. However, experimental observations of functional mitochondria in cancer cells have since refuted his hypothesis (Zong et al., 2016). In fact, increased glycolysis has been frequently verified in tumors, even in the presence of oxygen. It is now established that, cancer cells switch to glycolysis to supply their

bioRxiv preprint doi: https://doi.org/10.1101/2020.07.30.228759; this version posted July 30, 2020. The copyright holder for this preprint (which was not certified by peer review) is the author/funder. All rights reserved. No reuse allowed without permission.

increased need for biosynthetic precursors and organic resources to synthetize cell components (Vander Heiden et al., 2009). As glycolysis produces less ATP than oxidative phosphorylation, cancer cells compensate for this energy gap by up-regulating glucose transporters to import more glucose into the cell. Enhanced glycolysis also produces reducing equivalents and many glycolytic intermediates are diverted into the pentose phosphate pathway to produce NADPH (Metallo and Vander Heiden, 2013), allowing cancer cells to fight against reactive oxygen species and oxidative stress (Patra and Hay, 2014).

The switch to glycolysis in cancer cells is orchestrated by oncogenes and tumor suppressors (Razungles et al., 2013). Specifically, the tumor suppressor gene p53 favors oxidative phosphorylation over glycolysis, enhancing the production of reactive oxygen species, to imbalance redox status and promote cell death (Gomes et al., 2018; Humpton and Vousden, 2019). p53 directly inhibits glycolysis by blocking the expression of glucose transporters GLUT1, GLUT4 (Schwartzenberg-Bar-Yoseph et al., 2004) and GLUT3 (Kawauchi et al., 2008). p53 also acts as a biochemical cofactor by inhibiting the enzymatic activity of Glucose-6-phosphate dehydrogenase (G6PD), the first and rate-limiting enzyme of the pentose phosphate pathway (Jiang et al., 2011). Conversely, inactivating p53 reduces oxygen dependence and allows cancer cells to grow in oxygen-limited conditions, such as hypoxia.

bioRxiv preprint doi: https://doi.org/10.1101/2020.07.30.228759; this version posted July 30, 2020. The copyright holder for this preprint (which was not certified by peer review) is the author/funder. All rights reserved. No reuse allowed without permission.

Hypoxia induces the stability of hypoxia inducible factors (HIFs) that stimulate glycolysis in tumor cells and antagonize p53 in cancer cells. The direct binding of HIF-1α to p53 could account for their antagonizing (Sánchez-Puig et al., 2005). Although this interplay has been widely described, its direct influence on glycolysis needs further clarification (Amelio and Melino, 2015; Sermeus and Michiels, 2011).

The transcriptional coregulator RIP140 regulates the activity of various transcription factors, mainly inhibiting their transactivation ability by recruiting histone deacetylases (Augereau et al., 2006). RIP140 can also activate transcription through SP1 (Castet et al., 2006), or NF-κB (Zschiedrich et al., 2008) sites. Due to its wide interactome, RIP140 influences numerous physiological functions, such as mammary gland development, fertility and inflammation (Nautiyal, 2017). RIP140 is also a major regulator of energy homeostasis, regulating lipogenesis in the liver, lipid storage and thermogenesis in adipose tissues, mitochondrial integrity, and the formation of oxidative fibers in the muscle (Nautiyal, 2017). In addition, RIP140 inhibits glucose uptake by two distinct mechanisms: i) by reducing the trafficking of the GLUT4 carrier at the adipocyte and muscle cell membranes (Fritah, 2009; Ho and Wei, 2012; Ho et al., 2009) and ii) by blocking the expression of GLUT4 in adipocytes (Powelka et al., 2006).

bioRxiv preprint doi: https://doi.org/10.1101/2020.07.30.228759; this version posted July 30, 2020. The copyright holder for this preprint (which was not certified by peer review) is the author/funder. All rights reserved. No reuse allowed without permission.

We, and other groups, have also reported that RIP140 plays crucial roles in tumorigenesis, promoting (Aziz et al., 2015; Rosell et al., 2014; Yu et al., 2018) or impairing breast tumor cell proliferation (Docquier et al., 2010; Jalaguier et al., 2017). In colorectal cancers, RIP140 regulates the APC/β-catenin pathway and inhibits the proliferation of intestinal cells. Moreover, RIP140 acts as a tumor suppressor, high expression of RIP140 correlating with good prognosis of colorectal cancer patients (Cavaillès and Lapierre, 2014; Lapierre et al., 2014).

Despite its separately documented roles in glycolysis and cancer cell proliferation, it is still unknown whether RIP140 is actually involved in the metabolism of glucose in cancer cells, and, if so, whether this directly affects their proliferation. Also in this context, any potential RIP140 target genes remain to be identified, together with the underlying molecular mechanisms.

Here we characterized the proliferative and glycolytic status of cancer cells with RIP140 knockdown and of immortalized or transformed mouse embryonic fibroblasts from RIP140 knock-out (RIPKO) mice. We also evaluated the survival of RIP140-deficient cells after disrupting glycolysis. We identified RIP140 glycolytic target genes by transcriptional analysis and characterized the mechanism by which RIP140 regulates the glycolysis of cancer cells. We

bioRxiv preprint doi: https://doi.org/10.1101/2020.07.30.228759; this version posted July 30, 2020. The copyright holder for this preprint (which was not certified by peer review) is the author/funder. All rights reserved. No reuse allowed without permission.

show for the first time that RIP140 regulates the transcription of genes implicated in glycolysis to influence tumor growth.

bioRxiv preprint doi: https://doi.org/10.1101/2020.07.30.228759; this version posted July 30, 2020. The copyright holder for this preprint (which was not certified by peer review) is the author/funder. All rights reserved. No reuse allowed without permission.

Results

RIP140-deficiency promotes cell proliferation and tumor growth.

As mentioned above, opposite effects of RIP140 on human cancer cell proliferation have been described. Aiming to clarify this situation, we first evaluated the impact of RIP140 silencing on proliferation of breast (MCF7 and MDA-MB-436), prostate (DU145) and colon (RKO) cancer cell lines by MTT and xCELLigence assays.

After small interfering RNA (siRNA) knockdown with two separate siRNAs, we measured proliferation by xCELLigence real-time cell analysis. RIP140 silencing consistently increased cell proliferation(Fig. 1a-c and Supplementary Fig. 1a-e) confirming our previous results. Therefore, in our experimental conditions, knocking-down RIP140 expression robustly increased cancer cell proliferation.

To further test the role of RIP140 on cell proliferation, we studied the proliferation of mouse embryonic fibroblasts (MEFs) knock-out for the *Rip140* gene (RIPKO, Supplementary Fig. 1f). 3T3-immortalized RIPKO MEFs proliferated more than 3T3-immortalized MEFs expressing *Rip140* (WT), as shown by MTT and xCELLigence assays(Fig 1c and Supplementary Fig. 1g). Immortalized RIPKO cells expressed more the proliferation markers, Cyclin A and Phosphorylated Serine10-Histone 3, and were also richer in ATP (Fig. 1d and Supplementary

bioRxiv preprint doi: https://doi.org/10.1101/2020.07.30.228759; this version posted July 30, 2020. The copyright holder for this preprint (which was not certified by peer review) is the author/funder. All rights reserved. No reuse allowed without permission.

Fig. 1h). Immortalization is an important step in cellular transformation and tumorigenesis, in which primary MEFs gain the capacity to grow forever by bypassing cellular senescence. In contrast, transformation of primary MEFs by two cooperating oncogenes, such as SV40 and HRas/V12, results in a loss of contact inhibition, anchorage-independent growth, and tumor formation in nude mice. In SV40-HRas/V12-transformed MEFs, RIP140-deficiency increased the cell proliferation and the number of colonies as shown, respectively, by MTT and soft agar assays(Supplementary Fig. 1i, j).

As the above data built a strong case for a growth inhibitory role of RIP140, we wondered whether RIP140 could also impact tumor growth. We, therefore, xenografted transformed RIPKO MEFs into nude mice and found that, indeed, these tumors had enhanced growth (Fig. 1e and Supplementary Fig. 1k, l).

To confirm the role of RIP140 in the observed effects, we rescued RIP140 expression by generating stable MEFs expressing either GFP or human RIP140 (Supplementary Fig. 1m). Rescuing RIP140 expression inhibited cell proliferation, in both xCELLigence and MTT assays (Fig. 1f and Supplementary Fig. 1n), and reduced colony number (Fig. 1g and Supplementary Fig. 1o). These data demonstrated that RIP140 inhibits cell growth in tumor cells.

bioRxiv preprint doi: https://doi.org/10.1101/2020.07.30.228759; this version posted July 30, 2020. The copyright holder for this preprint (which was not certified by peer review) is the author/funder. All rights reserved. No reuse allowed without permission.

Although pro-proliferative effects have been described for RIP140, our findings push toward an anti-proliferative effect of RIP140 on cancer cell proliferation.

Inhibiting glycolysis reduces the growth advantage of RIP140-deficient cells.

RIP140 regulates the homeostasis of glucose, which is one of the major nutrients of growing cells. To determine the importance of glucose for RIP140-deficient cell growth, we first performed glucose starvation experiments. Lowering glucose concentrations affected RIPKO cell proliferation more than WT cells in the MTT assay (Fig. 2a, and Supplementary Fig. 2a). As shown in Supplementary Fig. 2b, the growth advantage of RIPKO cells observed in glucose-rich medium was abolished in the absence of glucose.

Upon glucose starvation, Chiaradonna *et al.* reported that transformed MEFs displayed morphological features of cell death (Chiaradonna et al., 2006). Upon glucose starvation, transformed RIPKO MEFs had more features of dead cells than WT cells, such as loss of plasma membrane integrity and cell fragmentation (Fig. 2b). Furthermore, we found that transformed RIPKO MEFs were more sensitive to glucose limitation than transformed WT MEFs as shown by MTT assay (Supplementary Fig. 2c). These data suggest that RIP140-deficiency triggers glucose starvation-induced cell death.

bioRxiv preprint doi: https://doi.org/10.1101/2020.07.30.228759; this version posted July 30, 2020. The copyright holder for this preprint (which was not certified by peer review) is the author/funder. All rights reserved. No reuse allowed without permission.

Next, we analyzed cell viability after treatment with the glycolysis inhibitors 2-deoxyglucose (2DG, Hexokinase inhibitor) and 3-Bromopyruvate (BrP, GAPDH inhibitor).

As for glucose starvation, 2DG treatment induced the loss of the RIPKO cell growth advantage, as shown by MTT assay (Fig. 2c). This result was confirmed using an xCELLigence assay (Supplementary Fig. 2d). Moreover, treating with BrP induced the same response (Supplementary Fig. e). Cell proliferation and ATP level were more reduced in RIPKO MEFs under 2DG treatment, as shown by MTT and xCELLigence assays and ATP measurement (Fig 2d, e and Supplementary Fig. 2f). Moreover, RIPKO cells formed no colonies in the presence of the drug (Supplementary Fig. 2g). In preclinical models, treating our xenografted nude mice with 2DG led to a greater reduction in volume of RIPKO than WT tumors (Fig 2f).Finally, both glycolysis inhibitors reduced the MDA-MB-436 cell viability more efficiently when RIP140 was silenced by siRNA (Fig. 2g).

Altogether, these results demonstrate that the growth advantage of RIP140-deficient cells is abolished when glycolysis is impaired. RIP140-deficient cells therefore rely on glycolysis to grow, suggesting that RIP140 inhibits cell proliferation by blocking glycolysis.

RIP140-deficiency enhances glycolysis in breast cancer cells.

bioRxiv preprint doi: https://doi.org/10.1101/2020.07.30.228759; this version posted July 30, 2020. The copyright holder for this preprint (which was not certified by peer review) is the author/funder. All rights reserved. No reuse allowed without permission.

Because these results suggested that RIP140 inhibits glycolysis in tumor cells, we characterized the glycolytic properties of RIP140-deficient cells. To do so, we performed Seahorse flux analysis that allow the measurement of the glucose-induced extracellular acidification rate, reflecting glycolysis. When basal extracellular acidification rate was set up as reference for each cell line, the addition of glucose changed this acidification rate more in RIPKO cells (Fig. 3a). Further, the glycolytic parameters provided by the Agilent Wave software, including glycolysis, glycolytic capacity and glycolysis reserve, were higher in RIPKO MEFs (Fig. 3b). The high glycolysis content of RIPKO cells was confirmed in transformed MEFs (Supplementary Fig. 3a). Furthermore, glucose consumption and lactate production were higher in RIPKO cells, confirming the Seahorse analysis (Supplementary Fig. 3b). We also demonstrated that glucose uptake was higher in immortalized and transformed RIPKO MEFs (Fig. 3c). Then, rescuing RIP140 expression reduced extracellular acidification, confirming the inhibitory effect of RIP140 on glycolysis (Fig. 3d).

Finally, silencing RIP140 by siRNA in human cancer cells increased glycolysis (Fig. 3e and Supplementary 3d). Thus, these results demonstrate for the first time that the loss of RIP140 increased glycolysis in cancer cells.

bioRxiv preprint doi: https://doi.org/10.1101/2020.07.30.228759; this version posted July 30, 2020. The copyright holder for this preprint (which was not certified by peer review) is the author/funder. All rights reserved. No reuse allowed without permission.

GLUT3 and G6PD are essential for the growth advantage of RIP140-deficient cells.

To investigate how RIP140 regulates glycolysis in cancer cells, we monitored the expression of 24 different metabolic genes involved in glycolysis by RT-qPCR in RIP140-deficient cells. The mRNA level of *GLUT3*, *GLUT4*, *LDHB* (Lactate Dehydrogenase B) and *G6PD* was above a 2-fold change threshold between RIPKO and WT immortalized MEFs (Supplementary Fig. 4a). The increase of *GLUT3* and *G6PD* mRNA expression level was recapitulated in transformed MEFs (Supplementary Fig. 4b). Furthermore, these two genes were also significantly increased by RIP140 silencing in the breast cancer cell lines MCF7 and MDA-MD-436 (Fig. 4a and Supplementary Fig. 4c), whereas the *LDHB* and *GLUT4* levels did not change significantly (data not shown). The induction of GLUT3 and G6PD was also confirmed at the protein level in MEFs (Fig. 4b and Supplementary Fig. 4d). Furthermore, rescuing RIP140 expression in RIPKO MEFs downregulated these two genes (Fig. 4c), suggesting that *Glut3* and *G6pd* might be involved in RIP140-regulated glycolysis.

G6PD is the first and rate-limiting enzyme of the pentose phosphate pathway. We evaluated its importance in RIP140-deficient cells by first quantifying its enzymatic activity. We found that G6PD activity was higher in RIPKO than in WT MEFs (Fig. 4d). As a correlate of the high G6PD activity, the NADPH/NADP+ ratio was higher in KO cells than in control cells

bioRxiv preprint doi: https://doi.org/10.1101/2020.07.30.228759; this version posted July 30, 2020. The copyright holder for this preprint (which was not certified by peer review) is the author/funder. All rights reserved. No reuse allowed without permission.

(Supplementary Fig. 4e). Moreover, RIP140-deficient cells were more sensitive to G6PD inhibition by 6-Aminonicotinamide than control cells, as shown by MTT and colony formation assays, suggesting that RIP140-deficient cells rely on the pentose phosphate pathway to grow (Fig. 4e, f and Supplementary Fig. 4f-h).

To test whether GLUT3 or G6PD are needed by RIP140-deficient cells, we knocked down these genes either with small hairpin RNA (shRNA) in MEFs or with siRNA in MDA-MB-436 (Supplementary Fig. 4i-k). Knocking down either *Glut3* or *G6pd* abrogated the growth advantage induced by RIP140-deficiency, in both cell types as shown by either colony formation or MTT assays (Fig. 4g, h and Supplementary Fig. 4l, m). Finally, interrogating the breast cancer database Breastmark allowed us to find that low ratios between RIP140 and GLUT3 or between RIP140 and G6PD were associated with poor prognosis in breast cancers (Fig. 4j). Altogether, these data show that RIP140-deficiency stimulates cell proliferation mainly through *GLUT3* and *G6PD* induction.

RIP140 and p53 interact to down-regulate GLUT3.

Next, we investigated the mechanism by which RIP140 inhibits *GLUT3* and *G6PD* expression. Performing luciferase reporter assays using the *GLUT3* promoter allowed us to

bioRxiv preprint doi: https://doi.org/10.1101/2020.07.30.228759; this version posted July 30, 2020. The copyright holder for this preprint (which was not certified by peer review) is the author/funder. All rights reserved. No reuse allowed without permission.

show that RIP140 knock-down increased the luciferase activity of this reporter (Fig 5a, b). The luciferase activity of the *G6PD* promoter was also enhanced by RIP140 knock-down (Supplementary Fig. 5a). These results were confirmed using transformed MEFs in a luciferase reporter assay (Supplementary Fig. 5b). Moreover, RIP140 overexpression decreased the luciferase activity of both reporters (Fig. 5b and Supplementary 5c). These data confirmed the transcriptional inhibition of RIP140 on GLUT3 and G6PD expression.

RIP140 is a transcriptional coregulator and not a direct DNA binding protein, but in certain conditions it could be found in the vicinity of target genes. Then, a chromatin immunoprecipitation (ChIP) assay in MDA-MB-436 cells revealed the recruitment of RIP140 to the *GLUT3* promoter, indicating that regulation by RIP140 occurred directly within the promoter region of *GLUT3* (Fig. 5c). We did not find RIP140 within the promoter region of *G6PD*, suggesting that RIP140 recruitment may occur elsewhere within the gene (data not shown). We therefore decided to focus on *GLUT3* regulation by RIP140.

One of the direct DNA binding factors that likely could mediate RIP140 activity is p53, as it is a well-known inhibitor of the Warburg effect (Gomes et al., 2018). Thus, we investigated whether p53 mediated any of the transcriptional activities of RIP140 on *GLUT3* expression. Using a luciferase reporter assay, we showed that increasing doses of p53 enforced the

bioRxiv preprint doi: https://doi.org/10.1101/2020.07.30.228759; this version posted July 30, 2020. The copyright holder for this preprint (which was not certified by peer review) is the author/funder. All rights reserved. No reuse allowed without permission.

inhibitory effect of RIP140 on the luciferase activity driven by the *GLUT3* promoter, and that both proteins cooperated to repress this luciferase activity (Fig 5d, e). We then wondered whether this cooperative inhibition relies on direct protein-protein interaction. A proximity ligation assay (PLA) using antibodies against both endogenous proteins revealed RIP140 and p53 in close proximity in WT cells (Fig 5f). Moreover, we discovered a direct interaction *in vitro* between both proteins by GST-pulldown (Fig 5g).

Strikingly, RIP140-deficiency also clearly down-regulated p53 expression at both protein and mRNA levels (Fig. 5h and Supplementary Fig. 5d). Consistently, rescuing RIP140 led to an increase in *p53* mRNA level (Supplementary Fig. 5e). Silencing RIP140 also down-regulated *p53* mRNA in MCF7 cells (Supplementary Fig. 5f). Overall then our data suggest that RIP140, not only interacts and synergizes with p53, but also regulates its expression.

RIP140 and p53 inhibit the expression of GLUT3 induced by HIF-2α.

The common thread of the above data from RIP140-deficient cells: p53 inactivation, enhanced glycolysis and cell proliferation, is that these are all hallmarks of hypoxia. Hypoxia induces the stability of hypoxia inducible factors, or HIFs, which have an oxygen sensitive α sub-unit (HIF-1α, HIF-2α or HIF-3α) and one stable β sub-unit (HIF-1β; also known as

bioRxiv preprint doi: https://doi.org/10.1101/2020.07.30.228759; this version posted July 30, 2020. The copyright holder for this preprint (which was not certified by peer review) is the author/funder. All rights reserved. No reuse allowed without permission.

ARNT)(Majmundar et al., 2010). Our findings indicated that RIP140 and p53 cooperated to inhibit *GLUT3* expression. Thus, we wondered whether this cooperation could target HIFs activity.

We first assessed the effect of RIP140 on the transcriptional activity of HIFs. Using a luciferase reporter assay, we found that the transcriptional activity of a reporter gene containing hypoxia-response elements was higher in RIPKO than in WT MEFs (Fig 6a). Increasing doses of RIP140 repressed the basic activity of this reporter gene, but also the luciferase activity induced by DFO treatment, which mimics hypoxia, suggesting that RIP140 repressed HIF activity (Fig. 6a). However, RIP140 did not repress the activity of the hypoxia-response element-luciferase promoter when activated by the ectopic expression of HIF-1α or HIF-2α at high doses, suggesting that another factor was required for RIP140 to repress HIF activity (Supplementary Fig. 6a).

To identify this other factor, we decided to look at p53, which is known to inhibit the transcriptional activity of HIFs (Blagosklonny et al., 1998). Indeed, in our luciferase reporter assays, p53 inhibited the transcriptional activity of HIF-1α and HIF-2α (Fig. 6b). Strikingly, this repressive activity was stronger when RIP140 and p53 were expressed together (Fig. 6b). These results demonstrate that RIP140 and p53 cooperate to inhibit HIF transcriptional activity.

bioRxiv preprint doi: https://doi.org/10.1101/2020.07.30.228759; this version posted July 30, 2020. The copyright holder for this preprint (which was not certified by peer review) is the author/funder. All rights reserved. No reuse allowed without permission.

As hypoxia is known to induce GLUT3 expression (Mimura et al., 2012), we next asked if hypoxia affects *Glut3* expression in RIPKO cells. Either DFO treatment or HIF overexpression both increased the level of *Glut3* mRNA in RIPKO but not in WT MEFs (Fig. 6c, d and Supplementary Fig. 6b). These results suggest that the physiological role of p53/RIP140 could be to block the up-regulation of GLUT3 by the HIFs.

To test this hypothesis, we first up-regulated the HIFs in a luciferase gene reporter driven by the *GLUT3* promoter. We found that the overexpression of HIF-2α, but not HIF-1α, increased the activity of the *GLUT3* promoter (Supplementary Fig. 6c). Consistent with a specific role for this family member, we found that HIF-2α, and not HIF-1α, was overexpressed in RIP140-deficient cells (Supplementary Fig. 6d-f). Interestingly, HIF-2α silencing reduced the expression of *Glut3*, only in RIP140 KO MEFs (Fig. 6e).

We then wondered whether HIF-2α participated in the proliferative advantage of RIP140-deficient cells. Silencing HIF-2α significantly reduced RIPKO cell proliferation, as shown by xCELLigence analysis of RIPKO MEFs expressing a specific HIF-2α siRNA (Fig. 6f). Finally, our hypothesis that p53/RIP140 impacts HIF-dependent induction of *GLUT3* expression was confirmed in a luciferase reporter assay. Indeed, RIP140 and p53 inhibited the expression of the *GLUT3* promoter induced by HIF-2α (Fig. 6g).

bioRxiv preprint doi: https://doi.org/10.1101/2020.07.30.228759; this version posted July 30, 2020. The copyright holder for this preprint (which was not certified by peer review) is the author/funder. All rights reserved. No reuse allowed without permission.

To further decipher the mechanism, we wondered whether or not the DNA binding function of p53 was required to inhibit the transcriptional activity of HIF-2 α. For this, we used the p53 mutant R273H, which cannot bind to DNA. Consistent with a non DNA-binding mechanism, the mutant p53 had the capacity to inhibit the basal activities of either a hypoxia-response element- or a *GLUT3*-dependent promoters. When HIF-2α was over-expressed, the mutant p53 still repressed the activity of both promoters (Fig. 6h).

The fact that p53 inhibition did not require its DNA binding, along with the fact that RIP140 and p53 interacted (Fig. 5) suggested that the interplay between RIP140, p53 and HIF-2α could be mediated through protein-protein interactions. Performing a proximity ligation assay demonstrated that HIF-2α interacted with RIP140 and p53, suggesting that the three proteins could be involved in a ternary complex (Fig. 6i and Supplementary Fig. 6g).

Discussion

Altogether our data reveal that RIP140 inhibits the glycolysis-dependent proliferation of cancer cells by coordinately impeding glycolysis and the pentose phosphate pathway through the blockade of *GLUT3* and *G6PD* expression. Moreover, RIP140 and p53 jointly inhibit the

bioRxiv preprint doi: https://doi.org/10.1101/2020.07.30.228759; this version posted July 30, 2020. The copyright holder for this preprint (which was not certified by peer review) is the author/funder. All rights reserved. No reuse allowed without permission.

expression of *GLUT3* induced by HIF-2α., This new model of the regulation of glycolysis in tumorigenesis is detailed in Figure 7.

Glycolysis is essential for supporting the rapid proliferation of tumor cells. Our results demonstrate that the gain in tumor cell proliferation caused by the decrease or loss of RIP140 expression is abolished by glucose deprivation or by glycolysis blockade, showing the glucose dependency of RIP140-deficient cells. Of note, transformed RIPKO cells were more sensitive to glucose starvation than immortalized MEFs, suggesting that RIP140-deficiency might influence the transformation process in cancer by regulating glycolysis (Fig. 2b and Supplementary Fig. 2a). Interestingly, RIP140 does not regulate the metabolism of glutamine although this amino acid is also important for the proliferation of cancer cells (Jin et al., 2016). Indeed, the proliferation of WT and RIP140 KO cells was equally impacted by glutamine deprivation (data not shown), suggesting that RIP140 specifically affects glycolysis.

We demonstrated that RIP140-deficiency induced p53 down-regulation and HIF-2α up-regulation. While we observed an opposite effect of RIP140 on p53 and HIF-2α expression in MEFs, this contrary regulation was not observed in the cancer cells that we studied. The status

bioRxiv preprint doi: https://doi.org/10.1101/2020.07.30.228759; this version posted July 30, 2020. The copyright holder for this preprint (which was not certified by peer review) is the author/funder. All rights reserved. No reuse allowed without permission.

of p53 was different in the cancer cell lines that we used; MDA-MB-436 cells have a p53 mutation whereas MCF7 cells are p53 wild type (Concin et al., 2003). However, we saw no correlation between p53 status and responses to RIP140 silencing. In RIPKO MEFs, where p53 is down-regulated and HIF-2α is stabilized, the loss of RIP140 provoked a mild-hypoxia status leading to glycolysis stimulation and cell survival. Evaluating the expression of the three partners in tumor samples could indicate whether they are localized within hypoxic regions. One can imagine that such specific tumor hypoxia biomarkers will be valuable in developing hypoxia-based therapies or treatment strategies.

Our tailored experiments did not uncover how RIP140 regulates the expression of G6PD, which will require further work to establish. By contrast, our study describes the mechanism of the regulation of *GLUT3* expression, which relies on the cooperation of RIP140 and p53 to inhibit the expression of *GLUT3* induced by HIF-2α (Fig. 6g). The DNA-binding-defective p53 R273H mutant still efficiently repressed the transcriptional activity of HIF-2 α, suggesting that the mechanism of this cross-talk likely involves protein-protein interactions (Fig. 6h). Indeed, proximity ligation assays allowed us to visualize the three partners in close proximity two-by-two, suggesting that they are involved in a ternary complex (Fig. 5f, 6i). Our data reveals for

bioRxiv preprint doi: https://doi.org/10.1101/2020.07.30.228759; this version posted July 30, 2020. The copyright holder for this preprint (which was not certified by peer review) is the author/funder. All rights reserved. No reuse allowed without permission.

the first time that RIP140 interacts with p53 and HIF. Whether there is a ternary complex or if the interactions follow a temporal order will need to be defined in future studies.

It is tempting to speculate that RIP140 could act as an integrator protein such as CBP/p300 as p53 and HIF antagonism relies on competition for p300 (Schmid et al., 2004). RIP140 could enter into the competition with CBP as it does for nuclear receptors (Chen et al., 2004). The interplay between p53 and HIFs, although widely studied, remains a complex question, however, and it is still debated whether or not their reciprocal influence has any direct consequences for metabolism in cancer. Our results add RIP140 as a new major player in this interplay, and provide an additional bond between cell metabolism and cancer progression.

Our results also revealed that RIP140 impacts both glycolysis and the pentose phosphate pathway. The proliferative advantage of RIP140-deficient cells was blocked by the pharmacological inhibition of each pathway separately. Furthermore, down-regulating *Glut3* or *G6pd* expression provoked the same inhibition of RIP140-deficient cell proliferation. Combining the inhibition of both glycolysis and the pentose phosphate pathway could therefore block the proliferation of RIP140-deficient cancer cells more strongly. The overexpression of

bioRxiv preprint doi: https://doi.org/10.1101/2020.07.30.228759; this version posted July 30, 2020. The copyright holder for this preprint (which was not certified by peer review) is the author/funder. All rights reserved. No reuse allowed without permission.

GLUT3 or *G6PD* has been described in many types of cancer with poor outcomes (Benito et al., 2017; Kuang et al., 2017). In breast cancer patients, we found that a high level of *RIP140* combined with low levels of *GLUT3* or *G6PD* was linked to a poor survival (Fig. 4i). Cellular metabolism in cancer is currently being targeted in clinical trials with some success (Sborov et al., 2015). Our results suggest that these ratios could be used to identify patients that could benefit of therapies targeting glycolysis and/or HIF inhibitors. Altogether, our results enable us to propose a new model explaining the transcriptional control of glycolysis-dependent cancer cell proliferation by a nuclear interplay between three actors.

bioRxiv preprint doi: https://doi.org/10.1101/2020.07.30.228759; this version posted July 30, 2020. The copyright holder for this preprint (which was not certified by peer review) is the author/funder. All rights reserved. No reuse allowed without permission.

Acknowledgements

We thank Dr. Yuan, Dr. Karadimitris and Prof. Schymkowitz for the kind gift of plasmids, and Drs. Lapierre and Palassin for the generation of immortalized MEF #1 and stable MEF#1 overexpressing hRIP140, respectively. Thanks also to Dr. Stallcup for proofreading the manuscript. We gratefully acknowledge the financial support of ARC Foundation (R15083FF), Ligue Contre le Cancer (LNCC R13008FF, LNCC R15016FF), and Fondation pour la Recherche Médicale (N° DEQ20170336713).

Author contributions

V.J., D.G., S.F., L.K.L., S.B., S.J. and C.T. performed the experiments. S.F. and L.K.L contributed to the in vivo experiments. S.F. generated MEF #2. V.J. and S.J. performed breast cancer cell proliferation experiments. V.J. performed ChIP experiments, glycolysis inhibition and siRNA experiments in cancer cells, NADP/NADPH ratio measurements, and glucose starvation experiments. D.G performed immunoblots, ATP measurement, 2DG treatment experiments, cell proliferation and G6PD activity assays in MEF#1. S.B. performed luciferase reporter assays and GST pull-down experiments. C.T. generated MEF #3 and #4, performed

bioRxiv preprint doi: https://doi.org/10.1101/2020.07.30.228759; this version posted July 30, 2020. The copyright holder for this preprint (which was not certified by peer review) is the author/funder. All rights reserved. No reuse allowed without permission.

Seahorse, glucose uptake, xCELLigence, soft agar, PLA, shRNA experiments, luciferase reporter assays and immunoblots. V.J, V.C. and C.T. designed the studies and interpreted the data. C.T. wrote the manuscript. V.C. reviewed and approved the manuscript. All authors discussed and revised the manuscript. V.J. was supported by a fellowship from the French Ministry of Research.

Data Availability

Source data for all the figures are provided with the paper. All materials are available upon request to the corresponding authors.

Competing Interests statement

The authors declare no competing financial interests.

bioRxiv preprint doi: https://doi.org/10.1101/2020.07.30.228759; this version posted July 30, 2020. The copyright holder for this preprint (which was not certified by peer review) is the author/funder. All rights reserved. No reuse allowed without permission.

Materials and Methods

Plasmids and reagents.

RIP140-expressing vectors (pEFcmyc-RIP140 (Carascossa et al., 2006), pEGFP-RIP140 (Zilliacus et al., 2001)) and control vectors, pEGFP (Clontech), are described elsewhere. HA-HIF1alpha-pcDNA3 (Addgene plasmid # 18949) and HA-HIF2alpha-pcDNA3 (Addgene plasmid # 18950) plasmids were gifts from Dr Kaelin (Kondo et al., 2002). The GLUT3-Luc and G6PD-Luc reporter genes were gifts from Dr. Yuan (Liu et al., 2014) and Dr. Karadimitris (Makarona et al., 2014), respectively. The pCDNA3-p53R273H vector was kindly donated by Prof. Schymkowitz (Xu et al., 2011). 2-Deoxy-D-glucose (2DG, D6134)), 6-Aminonicotinamide (6AN; # A68203), 3-Bromopyruvate (BrP; #16490), MTT ((3- (4,5-dimethylthiazol-2-yl)-2,5-diphenyl tetrazolium bromide) (98%, CAS 298-93-1), Deferoxamine mesylate salt (D9533), Di(N-succinimidyl) glutarate (80424), crystal violet (C0775), G6PDH Activity Assay Kit (MAK015), anti-Mouse IgG-FITC antibody (F6257), monoclonal Anti-ß-Actin-Peroxidase antibody (A3854) were purchased from Sigma-Aldrich (Merck, Darmstadt, Germany). Puromycin (ant-pr-1) was purchased from Invivogen (France). The ATP Determination Kit (10700345) was from Fisher Scientific (France). Deoxy-D-glucose, 2-[1,2-3H (N)] (NET328A250UC) was from Perkin Elmer (France). GLUT3 shRNA (m) (sc-41219-

bioRxiv preprint doi: https://doi.org/10.1101/2020.07.30.228759; this version posted July 30, 2020. The copyright holder for this preprint (which was not certified by peer review) is the author/funder. All rights reserved. No reuse allowed without permission.

V), G6PD shRNA (m) (sc-60668-V) were purchased from Santa Cruz Biotechnology (Dallas, USA). Rabbit polyclonal to RIP140 (ab42126) was from Abcam (Cambridge, UK). BrdU Hu-purified-clone B44 (#347580) was from Becton Dickinson (France). NADP/NADPH-Glo assay (G9081) was from Promega (France).

Cell culture. Immortalized and transformed mouse embryonic fibroblasts (MEFs) were cultured in F12/Dulbecco's modified Eagle's medium supplemented with 10% fetal calf serum, 1% Penicillin/Streptomycin, 1mM Sodium Pyruvate and 10mM HEPES. Primary MEFs were prepared from 13.5 day wild-type (WT) or RIPKO mouse embryos (White et al., 2000) and genotyped by PCR. All experiments on mice were performed in accordance with French guidelines (agreement n° 201603101538202). Four independently derived RIP140 WT and RIPKO MEF cell lines were established. Immortalized MEFs were obtained by sequential passage, according to the 3T3 protocol (Todaro and Green, 1963), or by infection with retrovirus expressing SV40. After immortalization, MEFs were transformed with retrovirus expressing H-RasV12. Virus production, infection and transfection were performed as previously described (Rodier et al., 2015). Stably infected cells were selected with Puromycin (2.5µg/ml) after SV40 virus infection and Hygromycin (65µg/ml) after H-RasV12 virus infection. Immortalized MEFs were transduced with lentiviral particles expressing shRNA

bioRxiv preprint doi: https://doi.org/10.1101/2020.07.30.228759; this version posted July 30, 2020. The copyright holder for this preprint (which was not certified by peer review) is the author/funder. All rights reserved. No reuse allowed without permission.

against murine GLUT3 (sc-41219-V) or G6PD (sc-145295-V) according to the manufacturer's protocol (Santa Cruz Biotechnology,). MEFs transfected with pEGFP or pEGFP-hRIP140 were cultured in the presence of 3.2µg/ml Puromycin, as the selection agent to establish stable cell lines. MCF7, PC3 and DU145 were cultured in F12/Dulbecco's modified Eagle's medium supplemented with 10% fetal calf serum, 1% Penicillin/Streptomycin. MDA-M-B436 and RKO were cultured in Dulbecco's Modified Eagle Medium (DMEM) + GlutaMax (Thermo Fisher Scientific; Waltham, MA), supplemented with 10% FBS and 1% Penicillin/Streptomycin.

Real-time qPCR. Real-time qPCR was conducted as previously described (Jalaguier et al., 2017). Briefly, total RNA was extracted from cells using the Quick RNA™ Miniprep kit (Zymo Research, Irvine, CA, USA) according to the manufacturer's instructions. cDNA was synthetized with 1 µg of RNA and the qScript cDNA master mix (Quanta Bio, Beverly, MA, USA). mRNA expression was determined with a quantitative real time PCR SYBR Green SensiFAST™ SYBR® No-ROX Kit (Bioline, London, UK) on a Light Cycler® 480 Instrument II (Roche Life Sciences). Relative expression levels for the mRNAs of interest were normalized to 28S or RS9 housekeeping genes. See Supplemental Table 1 for the list of primer sequences.

Protein detection.

bioRxiv preprint doi: https://doi.org/10.1101/2020.07.30.228759; this version posted July 30, 2020. The copyright holder for this preprint (which was not certified by peer review) is the author/funder. All rights reserved. No reuse allowed without permission.

Protein expression was quantified by western blot analysis using the following antibodies: anti-cyclin A (1:500 sc-751; Santa Cruz Biotechnology, Dallas, TX, USA), anti-Histone H3 (phospho Serine10) (1:2,000 ab14955; Abcam Cambridge, UK), anti-GLUT3 (1:10000 ab191071; Abcam), anti-G6PD (1:1000 ab993; Abcam), anti-p53 (1:1000 1C12; Cell Signaling Technology, Leiden, The Netherlands), anti-HIF-1α (1:1000 NB100-105; Novus Biologicals, LLC (Centennial, USA)), anti-HIF-2α/EPAS1 (1:1000 NB100-122; Novus Biologicals, LLC (Centennial, USA)), and anti-Actin-HRP (1:10000 A3854, Merck, Darmstadt, Germany). Immunofluorescence, proximity ligation assays (PLA) and GST-pull down were performed as described (Jalaguier et al., 2017).

Luciferase assay. For gene reporter assays, cells were plated in 96-well plates and transfected with JetPEI (Polyplus, Illkirch-Graffenstaden, France) according to the manufacturer's protocol. Data were expressed as relative firefly luciferase activity normalized to renilla activity. For all experiments, data were collected from at least three biological replicates.

Chromatin immunoprecipitation. Approximately one hundred and twenty million cells were harvested per experiment. Briefly, protein–DNA complexes were first cross-linked, using 2mM Di (N-succinimidyl) GLUTarate (DSG), for 50 min on a rotor, then the procedure was performed using High-Sentivity kit (Active Motif, Shanghai) and according to manufacturer's

bioRxiv preprint doi: https://doi.org/10.1101/2020.07.30.228759; this version posted July 30, 2020. The copyright holder for this preprint (which was not certified by peer review) is the author/funder. All rights reserved. No reuse allowed without permission.

protocol. Chromatin was sonicated for thirty seconds on ice followed by thirty seconds off, for a total of thirty minutes. Immunoprecipitations were performed with 30µg of protein-DNA complexes and 4µg of RIP140 antibody (Ab42126; Abcam). The purified DNAs were amplified with SYBR Green SensiFAST™ SYBR® No-ROX Kit (Bioline, London, UK) by real-time qPCR.

Cell proliferation analysis

MTT assay. Cell proliferation assays were performed using MTT as previously described (Jalaguier et al., 2017). Data were normalized to the absorbance value at day 1. Experiments were performed three times with at least sextuplets. For glucose starvation experiments, cells grew for 24 hours in complete media. Then cells were washed twice with PBS and starvation medium (DMEM5030 supplemented with 10% dialyzed FBS, 2mM Glutamine, 1% Penicillin/Streptomycin, HEPES 10mM, 1mM Sodium Pyruvate, 3.7g/l Sodium Bicarbonate) was added to the cells supplemented, or not, with indicated glucose concentrations.

xCELLigence analysis. The Real-time Cell Analyzer DP instrument (Agilent, Santa Clara, USA) was placed in a humidified incubator maintained at 37ºC with 5% CO_2. Cells were plated at 1500 cells/well into 16-well E-Plates. The impedance value of each well was automatically

bioRxiv preprint doi: https://doi.org/10.1101/2020.07.30.228759; this version posted July 30, 2020. The copyright holder for this preprint (which was not certified by peer review) is the author/funder. All rights reserved. No reuse allowed without permission.

monitored every hour for up to the indicated times by the xCELLigence system. Cell proliferation is represented by an index that reflects changes in electrical impedance matching to cellular coverage of the electrode sensors.

Soft agar colony assay. Soft agar experiments were performed as described previously (Rodier et al., 2015). Briefly, transformed MEFs (8.10^4 cells) were mixed with culture medium containing 0.4% agar and seeded into 6-well plates coated with 1% agar in F12/DMEM containing 10% FBS in at least triplicate. Medium was changed twice a week. After 20 days, colonies were stained with 0.5% crystal violet solution, photographed and counted with ImageJ software.

Mouse xenograft assays. Transformed MEF ($5.\ 10^5$ cells) were resuspended in 100 µl of RPMI medium (Thermo Fisher Scientific; Waltham, MA) and injected subcutaneously into the dorsal area of 4-6 week-old immuno-deficient athymic female mice (Charles River, Écully, France). After 10-14 days, tumor volumes were measured every 3-4 days with a caliper. Before reaching tumor volume limit point, fibrosarcomas were excised, photographed and weighed.

Metabolic measurements

bioRxiv preprint doi: https://doi.org/10.1101/2020.07.30.228759; this version posted July 30, 2020. The copyright holder for this preprint (which was not certified by peer review) is the author/funder. All rights reserved. No reuse allowed without permission.

Glucose uptake. One day after cell seeding at 50,000 cells/well into 24-w plates, cells were washed once with PBS and medium was replaced with low-glucose medium (DMEM5030 supplemented with 10% dialyzed FBS (Thermo Fisher Scientific, Waltham, MA), 2mM Glutamine, 1% Penicilline/Streptomycin, HEPES 10mM, 1mM Sodium Pyruvate, 3.7g/l Sodium Bicarbonate, 0.25mM Glucose). Then 1µCi/ml of Deoxy-D-glucose, 2-[1,2-3H(N)] (Perkin Elmer, Waltham, MA) was added for 30 minutes at room temperature. Cells were washed once with PBS and then lysed with 200µl of 1%SDS; 10mM Tris pH 7.5. 100µl was used to count radioactivity with a Perkin Elmer liquid scintillation analyzer Tri-Carb 2900TR and 5µl was used to quantify proteins for normalization.

Cellular ATP measurement. ATP content was determined using the ATP determination kit according to the manufacturer's instructions (Molecular Probes, Thermo Fisher Scientific,Waltham, MA). Cells were washed with iced-cold 1x PBS and extracted in an ATP-releasing buffer containing 100 mM potassium phosphate buffer at pH 7.8, 2 mM EDTA, 1 mM dithiothreitol, and 1% Triton X-100. Then, 5 µl of lysate was used for protein determination by the DC Protein Assay (Bio-Rad Laboratories, Hercules, CA). ATP levels were expressed in nM ATP per 10 µg protein units and then normalized with respect to the level in control samples.

bioRxiv preprint doi: https://doi.org/10.1101/2020.07.30.228759; this version posted July 30, 2020. The copyright holder for this preprint (which was not certified by peer review) is the author/funder. All rights reserved. No reuse allowed without permission.

Seahorse experiments. Extracellular acidification rate (measured in mpH/min) was monitored using an XFe24 extracellular flux analyzer from Seahorse Bioscience (Agilent, Santa Clara, CA) following the manufacturer's protocol. Experiments were carried out on confluent monolayers. Briefly, cells were seeded 24 hours before experiments at a density of 35,000 cells/well (24-well). Before starting measurements, cells were washed once with PBS and medium was replaced with Seahorse XF Base Medium supplemented with 2mM glutamine without glucose at pH 7.4) and were placed into a 37 °C non-CO2 incubator for 1 hour prior to the assay. Glucose, oligomycin, and 2-DG were diluted into XF24 media and loaded into the accompanying cartridge to achieve final concentrations of 10 mM, 1 µm, and 100 mM, respectively. Injections of the drugs into the medium occurred at the time points specified. Each cycle consisted of 3 min mixing, 3 min waiting and 3 min measuring. Data were transformed with Agilent Seahorse Wave software to export glycolysis parameters. Values were expressed after normalization to the protein content of each well and to the values just before glucose addition. Acidification rates were presented as the mean ± SD of 4 to 6 replicate wells.

NADP/NADPH assays. Five thousand MEFs were seeded per well in a 96-well plate in 50 µL of DMEM-F12. 24 hours later, the NADP/NADPH balance was measured by NADP/NADPH-Glo Assay (Promega, Madison, WI) according to manufacturer's protocol.

bioRxiv preprint doi: https://doi.org/10.1101/2020.07.30.228759; this version posted July 30, 2020. The copyright holder for this preprint (which was not certified by peer review) is the author/funder. All rights reserved. No reuse allowed without permission.

Glucose and Lactate assays. Cells were seeded in culture dishes and cultured for 8 h. The culture medium was then changed and cells were incubated for an additional 16 h. Subsequently, the culture medium was collected for determination of glucose concentration and lactate levels using a Glucose assay kit (Amplite ™ Glucose Quantitation Assay kit, AAT Bioquest, Sunnyvale, CA) and a Lactate assay kit (MAK064, Merck, Darmstadt, Germany) according to the manufacturer's instructions. Glucose consumption was calculated as the difference in glucose concentration between fresh medium and cell supernatant. Lactate production was determined as the difference in lactate concentration between cell supernatant and fresh medium. Data were normalized to final cell counts and time.

G6PD activity assay. G6PD activity was determined with a Glucose-6-Phosphate Dehydrogenase Assay Kit (MAK015, Merck, Darmstadt, Germany) according to the manufacturer's instructions using 10 µg protein. Protein extraction and quantification were performed as for ATP determination. G6PD activity was determined as milli-units/mL then normalized with respect to the activity in WT MEF samples.

bioRxiv preprint doi: https://doi.org/10.1101/2020.07.30.228759; this version posted July 30, 2020. The copyright holder for this preprint (which was not certified by peer review) is the author/funder. All rights reserved. No reuse allowed without permission.

Statistical analysis. Data are expressed as mean ± SD. Unless stated otherwise, statistical analysis was performed by a Mann-Whitney test using StatEL. The p values less than 0.05 were considered to be statistically significant (***$p < 0.001$, **$p<0.01$, *$p < 0.05$).

Table1. Murine primer sequences

Name	Sequence
ALD1-FOR	TTCGCCTACCCACCGGCGTA
ALD1-REV	GGTGGCAGTGCTTTCCTGGCA
ALDOC-FOR	ACCATATTGGGCTTGAGCAG
ALDOC-REV	CCTCAAACGTTGCCAGTATGT
ENO1-FOR	AAAGATCTCTCTGGCGTGGA
ENO1-REV	CTTAACGCTCTCCTCGGTGT
ENO3-FOR	GGACTCCAGGGGCAACCCCA
ENO3-REV	TGCTCGGAATCGACCCTTGGC
GAPDH-FOR	GTGCAGTGCCAGCCTCGTCC
GAPDH-REV	CAGGCGCCCAATACGGCCAA
GLUT1-FOR	GAGTGTGGTGGATGGGATG
GLUT1-REV	AACACTGGTGTCATCAACGC
GLUT2-FOR	GGCTAATTTCAGGACTGGTT
GLUT2-REV	AACCAGTCCTGAAATTAGCC
GLUT3-FOR	ATCGTGGCATAGATCGGTTC
GLUT3-REV	TCTCAGCAGCTCTCTGGGAT
GLUT4-FOR	CAGTGTTCCAGTCACTCGCT
GLUT4-REV	TTTTAAAACAAGATGCCGTCG
GPI1-FOR	AAAGTCCAATGGCTGACCAC

bioRxiv preprint doi: https://doi.org/10.1101/2020.07.30.228759; this version posted July 30, 2020. The copyright holder for this preprint (which was not certified by peer review) is the author/funder. All rights reserved. No reuse allowed without permission.

GPI1-REV	CACGGCCAAAGTGAAAGAGT
G6PD-FOR	TCC GAG ATA TAC CAG GCG AC
G6PD-REV	GGC TTC TTG GTC ATC ATC GT
HIF1-FOR	AAACTTCAGACTCTTTGCTTCG
HIF1-REV	CGGCGAGAACGAGAAGAA
HIF2-FOR	ATC ACG GGA TTT CTC CTT CC
HIF2-REV	GGT TAA GGA ACC CAG GTG CT
HK2-FOR	GGAACCGCCTAGAAATCTCC
HK2-REV	GGAGCTCAACCAAAACCAAG
LDHA-FOR	GCAACATTCACACCACTCCA
LDHA-REV	TCCGTTACCTGATGGGAGAG
LDHB-FOR	GCTGCAGGTCCATCATCTCT
LDHB-REV	GTTGGACAAGTGGGTATGGC
PDK2-FOR	TTCCATGATGTCCAGCAGAC
PDK2-REV	GATCAACCTGCTTCCTGACC
PDK1-FOR	TTACTCAGTGGAACACCGCC
PDK1-REV	GTTTATCCCCCGATTCAGGT
PDK3-FOR	GTTAGCCAGTCGCACAGGA
PDK3-REV	CGTCGCCACTGTCTATCAAA
PDK4-FOR	TGACAGGGCTTTCTGGTCTT
PDK4-REV	AGTGAACACTCCTTCGGTGC
PFK2-FOR	AATGAGTGTTGGGGAGTTGG
PFK2-REV	CAGAAGACTGCAACAGCAGC
PFK3-FOR	CCACCATCACAATCACGGT
PFK3-REV	CAGAGCCGGGTACAGAAGAT
PG1-FOR	GTTCTTCAATGGCACCGACT
PG1-REV	AGTGGGACTGAGCCCAAAAT
PGK1-FOR	CAGCCTTGATCCTTTGGTTG
PGK1-REV	CTGACTTTGGACAAGCTGGA
PKM2-FOR	GCCGCCTGGACATTGACTC
PKM2-REV	CCA TGAGAGAAATTCAGCCGAG

bioRxiv preprint doi: https://doi.org/10.1101/2020.07.30.228759; this version posted July 30, 2020. The copyright holder for this preprint (which was not certified by peer review) is the author/funder. All rights reserved. No reuse allowed without permission.

p53-FOR	GAAGTCCTTTGCCCTGAAC
p53-REV	CTAGCAGTTTGGGCTTTCC
TPI1-FOR	AAAGTCGATGTAAGCGGTGG
TPI1-REV	GAAGTGCCTGGGAGAACTCA

Table 2. ChIP primer sequences

Name	Séquence	Ref
NegCHIP-FOR	ATGGTTGCCACTGGGGATCT	(Liu et al., 2014)
NegCHIP-REV	TGCCAAAGCCTAGGGGAAGA.	(Liu et al., 2014)
GLUT3CHIP-FOR	CCCCTGAAGCAATCTTGTGATC	(Liu et al., 2014)
GLUT3CHIP-REV	AAAAA CCCAGGGTGGAGAGAG	(Liu et al., 2014)
humanG6PD Prom (For)	GGA AAC GGT CGT ACA CTT CG	(Gromak et al., 2013)
humanG6PD Prom (Rev)	CAA ACA GCG TGT ATT TTA CCG	(Gromak et al., 2013)

bioRxiv preprint doi: https://doi.org/10.1101/2020.07.30.228759; this version posted July 30, 2020. The copyright holder for this preprint (which was not certified by peer review) is the author/funder. All rights reserved. No reuse allowed without permission.

Table 3. siRNA sequences.

Name	sequence	Ref
siControl	(UAAUGUAUUGGAACGCAUA)TT	
siRIP140-1=#2	(AUACGAAUCUUCCUGAUGU)TT	
siRIP140-4=#1	(GAAGCGUGCUAACGAUAAA)TT	
siHIF1mouse	(AAAGGACAAGUCACCACAGGA)TT	(Mi et al., 2008)
siHIF2mouse	(AAGUCACCAGAACUUGUGCAC)TT	(Mi et al., 2008)

References

Amelio, I., and Melino, G. (2015). The p53 family and the hypoxia-inducible factors (HIFs): determinants of cancer progression. Trends Biochem. Sci. *40*, 425–434.

Augereau, P., Badia, E., Balaguer, P., Carascossa, S., Castet, A., Jalaguier, S., and Cavaillès, V. (2006). Negative regulation of hormone signaling by RIP140. J. Steroid Biochem. Mol. Biol. *102*, 51–59.

Aziz, M.H., Chen, X., Zhang, Q., DeFrain, C., Osland, J., Luo, Y., Shi, X., and Yuan, R. (2015). Suppressing NRIP1 inhibits growth of breast cancer cells in vitro and in vivo. Oncotarget *6*, 39714–39724.

Benito, A., Polat, I.H., Noé, V., Ciudad, C.J., Marin, S., and Cascante, M. (2017). Glucose-6-phosphate dehydrogenase and transketolase modulate breast cancer cell metabolic reprogramming and correlate with poor patient outcome. Oncotarget *8*, 106693–106706.

Blagosklonny, M.V., An, W.G., Romanova, L.Y., Trepel, J., Fojo, T., and Neckers, L. (1998). p53 inhibits hypoxia-inducible factor-stimulated transcription. J. Biol. Chem. *273*, 11995–11998.

Carascossa, S., Gobinet, J., Georget, V., Lucas, A., Badia, E., Castet, A., White, R., Nicolas, J.-C., Cavaillès, V., and Jalaguier, S. (2006). Receptor-interacting protein 140 is a repressor of the androgen receptor activity. Mol. Endocrinol. *20*, 1506–1518.

bioRxiv preprint doi: https://doi.org/10.1101/2020.07.30.228759; this version posted July 30, 2020. The copyright holder for this preprint (which was not certified by peer review) is the author/funder. All rights reserved. No reuse allowed without permission.

Castet, A., Herledan, A., Bonnet, S., Jalaguier, S., Vanacker, J.-M., and Cavaillès, V. (2006). Receptor-interacting protein 140 differentially regulates estrogen receptor-related receptor transactivation depending on target genes. Mol. Endocrinol. *20*, 1035–1047.

Cavaillès, V., and Lapierre, M. (2014). Regulation of intestinal homeostasis and tumorigenesis by the transcriptional coregulator RIP140. Mol Cell Oncol *1*, e960761.

Chen, Y., Hu, X., and Wei, L.-N. (2004). Molecular interaction of retinoic acid receptors with coregulators PCAF and RIP140. Mol. Cell. Endocrinol. *226*, 43–50.

Chiaradonna, F., Sacco, E., Manzoni, R., Giorgio, M., Vanoni, M., and Alberghina, L. (2006). Ras-dependent carbon metabolism and transformation in mouse fibroblasts. Oncogene *25*, 5391–5404.

Concin, N., Zeillinger, C., Tong, D., Stimpfl, M., König, M., Printz, D., Stonek, F., Schneeberger, C., Hefler, L., Kainz, C., et al. (2003). Comparison of p53 Mutational Status with mRNA and Protein Expression in a Panel of 24 Human Breast Carcinoma Cell Lines. Breast Cancer Research and Treatment *79*, 37–46.

Docquier, A., Harmand, P.-O., Fritsch, S., Chanrion, M., Darbon, J.-M., and Cavaillès, V. (2010). The transcriptional coregulator RIP140 represses E2F1 activity and discriminates breast cancer subtypes. Clin. Cancer Res. *16*, 2959–2970.

Fritah, A. (2009). Control of skeletal muscle metabolic properties by the nuclear receptor corepressor RIP140. Appl Physiol Nutr Metab *34*, 362–367.

Gomes, A.S., Ramos, H., Soares, J., and Saraiva, L. (2018). p53 and glucose metabolism: an orchestra to be directed in cancer therapy. Pharmacol. Res. *131*, 75–86.

Gromak, N., Dienstbier, M., Macias, S., Plass, M., Eyras, E., Cáceres, J.F., and Proudfoot, N.J. (2013). Drosha Regulates Gene Expression Independently of RNA Cleavage Function. Cell Rep *5*, 1499–1510.

Ho, P.-C., and Wei, L.-N. (2012). Biological activities of receptor-interacting protein 140 in adipocytes and metabolic diseases. Curr Diabetes Rev *8*, 452–457.

Ho, P.-C., Lin, Y.-W., Tsui, Y.-C., Gupta, P., and Wei, L.-N. (2009). A negative regulatory pathway of GLUT4 trafficking in adipocyte: new function of RIP140 in the cytoplasm via AS160. Cell Metab. *10*, 516–523.

Hsu, P.P., and Sabatini, D.M. (2008). Cancer cell metabolism: Warburg and beyond. Cell *134*, 703–707.

Humpton, T., and Vousden, K.H. (2019). Taking up the reins of power: metabolic functions of p53. 610–614.

Jalaguier, S., Teyssier, C., Nait Achour, T., Lucas, A., Bonnet, S., Rodriguez, C., Elarouci, N., Lapierre, M., and Cavaillès, V. (2017). Complex regulation of LCoR signaling in breast cancer cells. Oncogene *36*, 4790–4801.

Jiang, P., Du, W., Wang, X., Mancuso, A., Gao, X., Wu, M., and Yang, X. (2011). p53 regulates biosynthesis through direct inactivation of glucose-6-phosphate dehydrogenase. Nat. Cell Biol. *13*, 310–316.

Jin, L., Alesi, G.N., and Kang, S. (2016). Glutaminolysis as a target for cancer therapy. Oncogene *35*, 3619–3625.

bioRxiv preprint doi: https://doi.org/10.1101/2020.07.30.228759; this version posted July 30, 2020. The copyright holder for this preprint (which was not certified by peer review) is the author/funder. All rights reserved. No reuse allowed without permission.

Kawauchi, K., Araki, K., Tobiume, K., and Tanaka, N. (2008). p53 regulates glucose metabolism through an IKK-NF-kappaB pathway and inhibits cell transformation. Nat. Cell Biol. *10*, 611–618.

Kondo, K., Klco, J., Nakamura, E., Lechpammer, M., and Kaelin, W.G. (2002). Inhibition of HIF is necessary for tumor suppression by the von Hippel-Lindau protein. Cancer Cell *1*, 237–246.

Kuang, R., Jahangiri, A., Mascharak, S., Nguyen, A., Chandra, A., Flanigan, P.M., Yagnik, G., Wagner, J.R., Lay, M.D., Carrera, D., et al. (2017). GLUT3 upregulation promotes metabolic reprogramming associated with antiangiogenic therapy resistance. JCI Insight *2*.

Lapierre, M., Bonnet, S., Bascoul-Mollevi, C., Ait-Arsa, I., Jalaguier, S., Del Rio, M., Plateroti, M., Roepman, P., Ychou, M., Pannequin, J., et al. (2014). RIP140 increases APC expression and controls intestinal homeostasis and tumorigenesis. J. Clin. Invest. *124*, 1899–1913.

Liu, X.-S., Haines, J.E., Mehanna, E.K., Genet, M.D., Ben-Sahra, I., Asara, J.M., Manning, B.D., and Yuan, Z.-M. (2014). ZBTB7A acts as a tumor suppressor through the transcriptional repression of glycolysis. Genes Dev. *28*, 1917–1928.

Majmundar, A.J., Wong, W.J., and Simon, M.C. (2010). Hypoxia-Inducible Factors and the Response to Hypoxic Stress. Molecular Cell *40*, 294–309.

Makarona, K., Caputo, V.S., Costa, J.R., Liu, B., O'Connor, D., Iskander, D., Roper, D., Robertson, L., Bhatnagar, N., Terpos, E., et al. (2014). Transcriptional and epigenetic basis for restoration of G6PD enzymatic activity in human G6PD-deficient cells. Blood *124*, 134–141.

Metallo, C.M., and Vander Heiden, M.G. (2013). Understanding Metabolic Regulation and Its Influence on Cell Physiology. Molecular Cell *49*, 388–398.

Mi, Z., Rapisarda, A., Taylor, L., Brooks, A., Creighton-Gutteridge, M., Melillo, G., and Varesio, L. (2008). Synergystic induction of HIF-1alpha transcriptional activity by hypoxia and lipopolysaccharide in macrophages. Cell Cycle *7*, 232–241.

Mimura, I., Nangaku, M., Kanki, Y., Tsutsumi, S., Inoue, T., Kohro, T., Yamamoto, S., Fujita, T., Shimamura, T., Suehiro, J., et al. (2012). Dynamic Change of Chromatin Conformation in Response to Hypoxia Enhances the Expression of GLUT3 (SLC2A3) by Cooperative Interaction of Hypoxia-Inducible Factor 1 and KDM3A. Molecular and Cellular Biology *32*, 3018–3032.

Nautiyal, J. (2017). Transcriptional coregulator RIP140: an essential regulator of physiology. J. Mol. Endocrinol. *58*, R147–R158.

Patra, K.C., and Hay, N. (2014). The pentose phosphate pathway and cancer. Trends Biochem. Sci. *39*, 347–354.

Powelka, A.M., Seth, A., Virbasius, J.V., Kiskinis, E., Nicoloro, S.M., Guilherme, A., Tang, X., Straubhaar, J., Cherniack, A.D., Parker, M.G., et al. (2006). Suppression of oxidative metabolism and mitochondrial biogenesis by the transcriptional corepressor RIP140 in mouse adipocytes. J. Clin. Invest. *116*, 125–136.

Razungles, J., Cavaillès, V., Jalaguier, S., and Teyssier, C. (2013). [The Warburg effect: from theory to therapeutic applications in cancer]. Med Sci (Paris) *29*, 1026–1033.

bioRxiv preprint doi: https://doi.org/10.1101/2020.07.30.228759; this version posted July 30, 2020. The copyright holder for this preprint (which was not certified by peer review) is the author/funder. All rights reserved. No reuse allowed without permission.

Rodier, G., Kirsh, O., Baraibar, M., Houlès, T., Lacroix, M., Delpech, H., Hatchi, E., Arnould, S., Severac, D., Dubois, E., et al. (2015). The transcription factor E4F1 coordinates CHK1-dependent checkpoint and mitochondrial functions. Cell Rep *11*, 220–233.

Rosell, M., Nevedomskaya, E., Stelloo, S., Nautiyal, J., Poliandri, A., Steel, J.H., Wessels, L.F.A., Carroll, J.S., Parker, M.G., and Zwart, W. (2014). Complex formation and function of estrogen receptor α in transcription requires RIP140. Cancer Res. *74*, 5469–5479.

Sánchez-Puig, N., Veprintsev, D.B., and Fersht, A.R. (2005). Binding of Natively Unfolded HIF-1α ODD Domain to p53. Molecular Cell *17*, 11–21.

Sborov, D.W., Haverkos, B.M., and Harris, P.J. (2015). Investigational cancer drugs targeting cell metabolism in clinical development. Expert Opin Investig Drugs *24*, 79–94.

Schmid, T., Zhou, J., Köhl, R., and Brüne, B. (2004). p300 relieves p53-evoked transcriptional repression of hypoxia-inducible factor-1 (HIF-1). Biochem. J. *380*, 289–295.

Schwartzenberg-Bar-Yoseph, F., Armoni, M., and Karnieli, E. (2004). The Tumor Suppressor p53 Down-Regulates Glucose Transporters GLUT1 and GLUT4 Gene Expression. Cancer Res *64*, 2627–2633.

Sermeus, A., and Michiels, C. (2011). Reciprocal influence of the p53 and the hypoxic pathways. Cell Death Dis *2*, e164.

Todaro, G.J., and Green, H. (1963). Quantitative studies of the growth of mouse embryo cells in culture and their development into established lines. J. Cell Biol. *17*, 299–313.

Vander Heiden, M.G., Cantley, L.C., and Thompson, C.B. (2009). Understanding the Warburg effect: the metabolic requirements of cell proliferation. Science *324*, 1029–1033.

White, R., Leonardsson, G., Rosewell, I., Ann Jacobs, M., Milligan, S., and Parker, M. (2000). The nuclear receptor co-repressor nrip1 (RIP140) is essential for female fertility. Nat. Med. *6*, 1368–1374.

Xu, J., Reumers, J., Couceiro, J.R., De Smet, F., Gallardo, R., Rudyak, S., Cornelis, A., Rozenski, J., Zwolinska, A., Marine, J.-C., et al. (2011). Gain of function of mutant p53 by coaggregation with multiple tumor suppressors. Nature Chemical Biology *7*, 285–295.

Yu, X.-H., Xue, X., Zhu, X., and Li, X. (2018). Downregulation of RIP140 in triple-negative breast cancer inhibits the growth and proliferation of cancer cells. Oncol Lett *15*, 8784–8788.

Zilliacus, J., Holter, E., Wakui, H., Tazawa, H., Treuter, E., and Gustafsson, J.A. (2001). Regulation of glucocorticoid receptor activity by 14--3-3-dependent intracellular relocalization of the corepressor RIP140. Mol. Endocrinol. *15*, 501–511.

Zong, W.-X., Rabinowitz, J.D., and White, E. (2016). Mitochondria and Cancer. Molecular Cell *61*, 667–676.

Zschiedrich, I., Hardeland, U., Krones-Herzig, A., Berriel Diaz, M., Vegiopoulos, A., Müggenburg, J., Sombroek, D., Hofmann, T.G., Zawatzky, R., Yu, X., et al. (2008). Coactivator function of RIP140 for NFkappaB/RelA-dependent cytokine gene expression. Blood *112*, 264–276.

bioRxiv preprint doi: https://doi.org/10.1101/2020.07.30.228759; this version posted July 30, 2020. The copyright holder for this preprint (which was not certified by peer review) is the author/funder. All rights reserved. No reuse allowed without permission.

Figure Legends.

Fig. 1. RIP140-deficiciency enhances cell proliferation and tumorigenesis.

a, b, Cell proliferation of breast cancer cells MCF7 (**a**) and (MDA-MB-436) (**b**) monitored by xCELLigence after silencing RIP140 by siRNA (representative experiment, n=2 independent experiments).

c, Cell proliferation of RIP140 WT and KO-immortalized MEFs (MEF #1) measured by MTT assay (n=4 independent experiments).

d, Western blot showing expression of Cyclin A, Phospho Serine 10-Histone 3 and Actin in MEF #1. Unprocessed original scans of blots are shown in Supplementary Figure 7.

e, SV40/H-RasV12-transformed MEF (MEF #2) WT and RIPKO cells were injected subcutaneously into the flanks of immuno-deficient mice (n=7) to assess their tumorigenic potential (left panel). The weight of the tumors were assessed six weeks after grafting (n=6 mice)(right panel).

f, Cell proliferation monitored by xCELLigence of MEF #1 WT stably overexpressing a pEGFP plasmid (WT+GFP) and (RIPKO+GFP) or a pEGFP-hRIP140 plasmid (RIPKO+hRIP140) (n=2 independent experiments).

bioRxiv preprint doi: https://doi.org/10.1101/2020.07.30.228759; this version posted July 30, 2020. The copyright holder for this preprint (which was not certified by peer review) is the author/funder. All rights reserved. No reuse allowed without permission.

g, Number of colonies of H-RasV12-transformed MEF #1 stably overexpressing pEGFP or pEGFP-hRIP140 obtained in a colony formation soft agar assay (representative experiment, n=4 independent experiments).

Fig. 2. Inhibiting glycolysis reduces the growth advantage of RIP140-deficient cells.

Unless otherwise stated, MEF #1 were used.

a, Cells were grown in medium whithout glucose. Cell proliferation analyzed by MTT assay was expressed relative to that of cells grown in Glucose 4.5g/L at day ten (representative experiment, n=3 independent experiments).

b, Microscopic morphological analysis of representative transformed MEF #3.

c, Cell proliferation analyzed by MTT assay upon 2-deoxyglucose treatment (2DG; 5mM) (n=3 independent experiments).

d, Cell number as percent of control following eight days of 2DG treatment (5mM) (n=3 independent experiments).

e, Cellular ATP content in MEF #1 after 3 days of 2DG treatment (5mM) expressed as percent of control (n=3 independent experiments).

bioRxiv preprint doi: https://doi.org/10.1101/2020.07.30.228759; this version posted July 30, 2020. The copyright holder for this preprint (which was not certified by peer review) is the author/funder. All rights reserved. No reuse allowed without permission.

f, Tumor volume of transformed MEF #1 xenografted in nude mice (n=6) after eighteen days of 2DG (20mg/g) administrated intra-peritoneally every other day.

g, Cell viability assessed by crystal violet staining of MDA-MB-436 after RIP140 silencing by siRNA at day seven and represented as percent of control after 2DG (5mM) and BrP (100µM) treatments (n=3 independent experiments).

Fig. 3. RIP140-deficiency enhances glycolysis in breast cancer cells.

Unless otherwise stated MEF #1 were used.

a, Percentage change in extracellular acidification rate (ECAR) was monitored in real-time with a Seahorse Bioscience Flux Analyzer. Cells were treated sequentially with glucose (10 mM), oligomycin (1µM) and 2-DG (100 mM). Values were normalized by protein quantity (representative experiment, n=5 independent experiments).

b, XF Glycolysis Stress Test Parameters represented as percent of basal WT ECAR from data obtained in Fig. 3a.

c, [^{3}H] 2-Deoxy-D-glucose uptake in MEF #1, #2 and #3, relative to the WT group and normalized by protein quantity (representative experiment, n=2 independent experiments).

bioRxiv preprint doi: https://doi.org/10.1101/2020.07.30.228759; this version posted July 30, 2020. The copyright holder for this preprint (which was not certified by peer review) is the author/funder. All rights reserved. No reuse allowed without permission.

d, Glycolysis represented by ΔECAR calculated as the difference of ECAR between basal and after-glucose injection in MEF #1 overexpressing or not hRIP140 (representative experiments, n=3 independent experiments).

e, Glycolysis represented by ΔECAR calculated as the difference of ECAR between basal and after-glucose injection after RIP140 silencing by siRNA (siRIP#2) in breast cancer cell lines MCF7 and MDA-MB-436 (representative experiments, n=3 independent experiments).

Fig. 4. GLUT3 and G6PD are essential for the growth advantage induced by RIP140-deficiency.

a, mRNA levels of *RIP140*, *GLUT3* and *G6PD* quantified by RT-qPCR in MDA-MB-436 after RIP140 silencing by siRNA (n=3 independent experiments).

b, Protein expression level of GLUT3, G6PD and Actin quantified by western blot in MEF #1. Unprocessed original scans of blots are shown in Supplementary Figure 7.

c, mRNA levels of *GLUT3* and *G6PD* quantified by RT-qPCR in MEF #1 overexpressing hRIP140 (n=3 independent experiments).

d, Relative G6PD activity quantified in MEF #1 with a G6PD assay kit (Sigma) (n=2 independent experiments).

bioRxiv preprint doi: https://doi.org/10.1101/2020.07.30.228759; this version posted July 30, 2020. The copyright holder for this preprint (which was not certified by peer review) is the author/funder. All rights reserved. No reuse allowed without permission.

e, MTT assay at day four in MEF #3 upon 6-aminonicotinamide treatment (6AN) (representative experiment, n=3 independent experiments).

f, Numbers of colonies obtained in colony formation soft agar assay of MEF #3 after three weeks of 6-aminonicotinamide (6AN) (10µM) treatment and represented as percent of control (n=3 independent experiments).

g, Number of colonies formed by transformed MEF #1 stably expressing shGLUT3 or shG6PD and expressed as percent of WT shControl (shC) (n=2 independent experiments).

h, Cell proliferation measured by MTT assay of MDA-MB-436 breast cancer cells after RIP140 siRNA silencing combined with siRNA GLUT3 or G6PD silencing (representative experiment, n=3 independent experiments). The proliferation of siRIP140 cells (siRIP) was expressed as relative to that of siControl cells (siC) for each conditions.

i, Expression in the opposite directions between RIP140 and GLUT3 (left panel) (4580 breast cancer samples) and patient survival using the BreastMark algorithm to perform on-line Kaplan–Meier analyses of several data sets (median cut-off). Expression in the opposite directions between RIP140 and G6PD (right panel) (4406 breast cancer samples) and patient survival using the BreastMark algorithm. The *P*-values are indicated. The blue line corresponds

bioRxiv preprint doi: https://doi.org/10.1101/2020.07.30.228759; this version posted July 30, 2020. The copyright holder for this preprint (which was not certified by peer review) is the author/funder. All rights reserved. No reuse allowed without permission.

to highRIP140/lowGLUT3 or highRIP140/lowG6PD. The red line corresponds to the opposite ratios.

Fig. 5. RIP140 and p53 interact to inhibit the expression of GLUT3.

a, Transient transfection in MDA-MB-436 cells co-transfected with the gene reporter GLUT3-Luc expressing the firefly luciferase in presence of increasing concentrations of a siRNA specific of RIP140 (siRIP#2). Relative luciferase units (RLU) values as readout (n=3 independent experiments).

b, Transient transfection in MEF #1 co-transfected with a GLUT3-Luc reporter gene in the presence of increasing concentrations of a RIP140-expressing plasmid (representative experiment, n=5 independent experiments).

c, Chromatin immunoprecipitation with anti-RIP140 or IgG in MDA-MB-436. Bound DNA was amplified by qPCR with GLUT3 promoter-specific primers as indicated (n=3 independent experiments).

d, Transient transfection in MEF #1 RIPKO co-transfected with a GLUT3-Luc reporter gene in the presence of a RIP140-expressing plasmid (50ng) and increasing concentrations of a p53-expressing plasmid (representative experiment, n=3 independent experiments).

bioRxiv preprint doi: https://doi.org/10.1101/2020.07.30.228759; this version posted July 30, 2020. The copyright holder for this preprint (which was not certified by peer review) is the author/funder. All rights reserved. No reuse allowed without permission.

e, Transient transfection in MEF #1 RIPWT co-transfected with a GLUT3-Luc reporter gene in the presence (or not) of both RIP140-expressing (100ng) and p53-expressing plasmids (50ng) (representative experiment, n=3 independent experiments).

f, Proximity ligation assay in MEF WT or p53 null cells between RIP140 and p53 using rabbit anti-RIP140 and mouse anti-p53 to detect endogenous proteins. Right panel: Dots were quantified with the Duolink Software from 5 independent microscopic fields.

g, GST pull-down assays using bacterially expressed GST and GST-RIP140 fragments and ^{35}S-labeled p53. Schematic representation of full-length RIP140 structure and p53 binding sites are indicated (site 1 and site 2). RD: Repression domain.

h, p53 protein levels in MEF #1 quantified by western blot (left panel) and mRNA level quantified by RT-qPCR (right panel: n= 4 independent experiments).

Fig. 6. RIP140 and p53 inhibit the expression of GLUT3 induced by HIF-2α.

a, Transient transfection in MEF #1 transfected with a Hypoxia Response Element reporter gene (HRE-Luc). DFO (0.1mM) was applied 24 h after transfection for 24 hours before performing luciferase assays (representative experiment, n=3 independent experiments).

bioRxiv preprint doi: https://doi.org/10.1101/2020.07.30.228759; this version posted July 30, 2020. The copyright holder for this preprint (which was not certified by peer review) is the author/funder. All rights reserved. No reuse allowed without permission.

b, Transient transfection in MEF #1 WT co-transfected with a HRE-Luc in presence of a HIF-1α-expressing plasmid and increasing concentrations of a RIP140-expressing plasmid in the presence of a p53-expressing plasmid (left panel, representative experiment, n=3 independent experiments). Transient transfection in MCF7 co-transfected with a HRE-Luc in presence of a HIF-2α-expressing plasmid and increasing concentrations of a RIP140-expressing plasmid in the presence of a p53-expressing plasmid (right panel, representative experiment, n=3 independent experiments).

c, *GLUT3* mRNA level quantified by RT-qPCR in MEF #1 after treatment with 0.1mM DFO for four hours. Samples were collected 48 h after DFO treatment (representative experiment, n=4 independent experiments).

d, *GLUT3* mRNA level quantified by RT-qPCR in MEF #1 transfected with plasmids expressing human HIF-1α or human HIF-2α for 48 h (representative experiment, n=3 independent experiments).

e, *GLUT3* mRNA level quantified by RT-qPCR in MEF #1 48h after HIF-2α siRNA silencing (n=3 independent experiments).

f, Cell proliferation monitored by xCELLigence of MEF #1 RIPKO after HIF-2α siRNA silencing (n=2 independent experiments).

bioRxiv preprint doi: https://doi.org/10.1101/2020.07.30.228759; this version posted July 30, 2020. The copyright holder for this preprint (which was not certified by peer review) is the author/funder. All rights reserved. No reuse allowed without permission.

g, Transient transfection in MEF #1 RIPKO co-transfected with a GLUT3-Luc reporter gene and increasing concentrations of a HIF-2α-expressing plasmid in the presence of a RIP140-expressing plasmid combined or not with a p53-expressing plasmid (representative experiment, n=3 independent experiments).

h, Transient transfection in MEF #1 RIPKO co-transfected with a HRE-Luc (left panel) or a GLUT3-Luc (right panel) and plasmids expressing either p53 WT or p53 R273H mutant in combination with a HIF-2α-expressing plasmid (representative experiment, n=3 independent experiments).

i, Proximity ligation assay in MEF #1WT between endogenous RIP140 and HIF-2α with rabbit anti-RIP140 and mouse anti-HIF-2α and between endogenous p53 and HIF-2α with rabbit anti-HIF-2α and mouse anti-p53.

Fig. 7. Model: RIP140 inhibits tumorigenesis by impacting the pentose phosphate pathway and glycolysis through the blockade of G6PD and GLUT3 expression. RIP140 and p53 together inhibit the expression of the GLUT3 promoter induced by HIF-2α. Green arrows indicate a

bioRxiv preprint doi: https://doi.org/10.1101/2020.07.30.228759; this version posted July 30, 2020. The copyright holder for this preprint (which was not certified by peer review) is the author/funder. All rights reserved. No reuse allowed without permission.

stimulating effect. Red lines indicate an inhibitory effect. Blue lines represent the cell membrane. Burgundy arrows represents the enzymatic reactions of glycolysis and the pentose phosphate pathway. Ovoid forms represent proteins. Green rectangle represent GLUT3 gene and green squares represent GLUT3 protein at the cell membrane. PPP stands for pentose phosphate pathway.

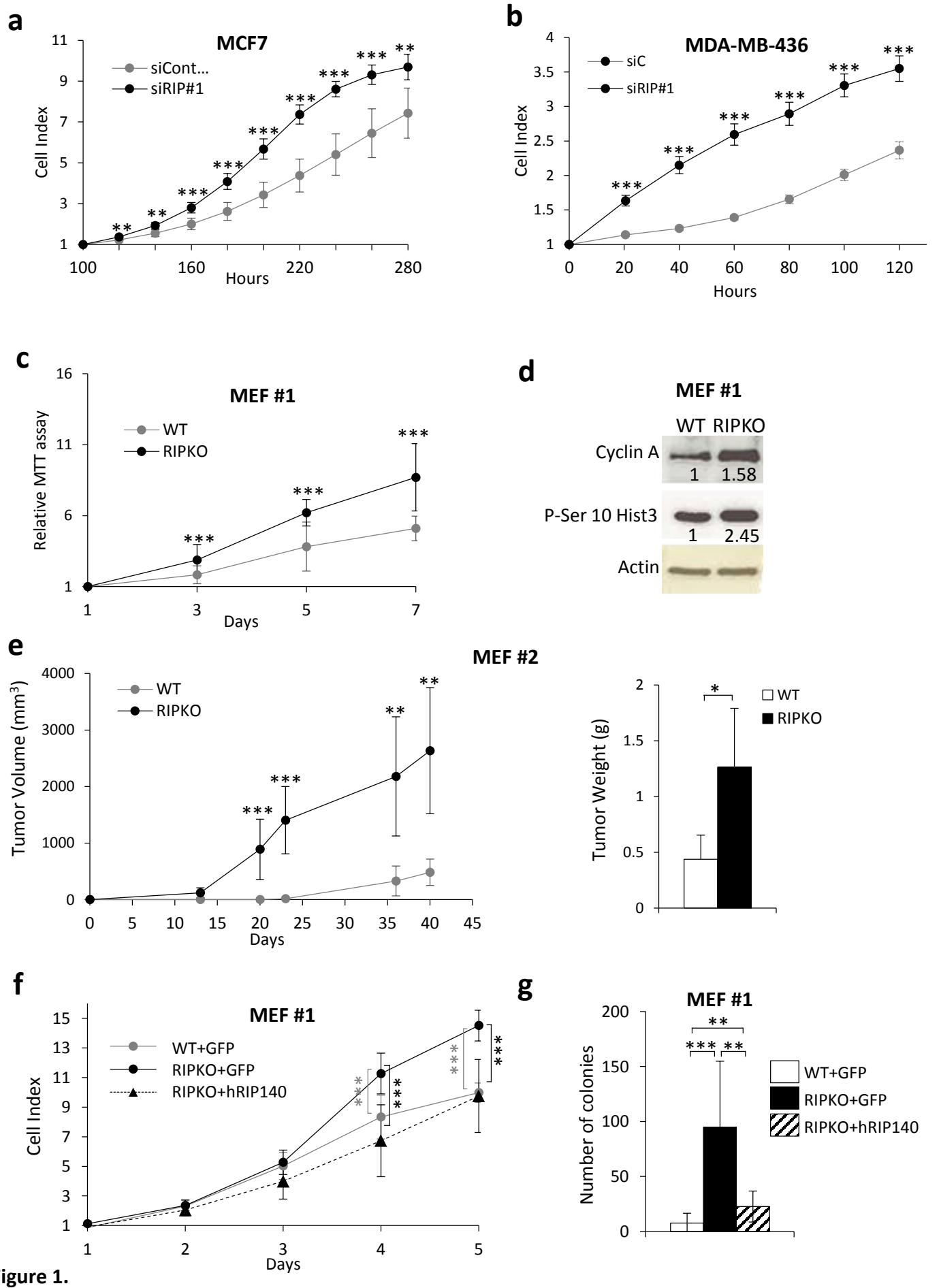
a
MCF7
siCont…
siRIP#1
Cell Index
Hours
b
MDA-MB-436
siC
siRIP#1
Cell Index
Hours
c
MEF #1
WT
RIPKO
Relative MTT assay
Days
d
MEF #1
WT RIPKO
Cyclin A
1 1.58
P-Ser 10 Hist3
1 2.45
Actin
e
MEF #2
WT
RIPKO
Tumor Volume (mm3)
Days
Tumor Weight (g)
WT
RIPKO
f
MEF #1
WT+GFP
RIPKO+GFP
RIPKO+hRIP140
Cell Index
Days
g
MEF #1
Number of colonies
WT+GFP
RIPKO+GFP
RIPKO+hRIP140

Figure 1.

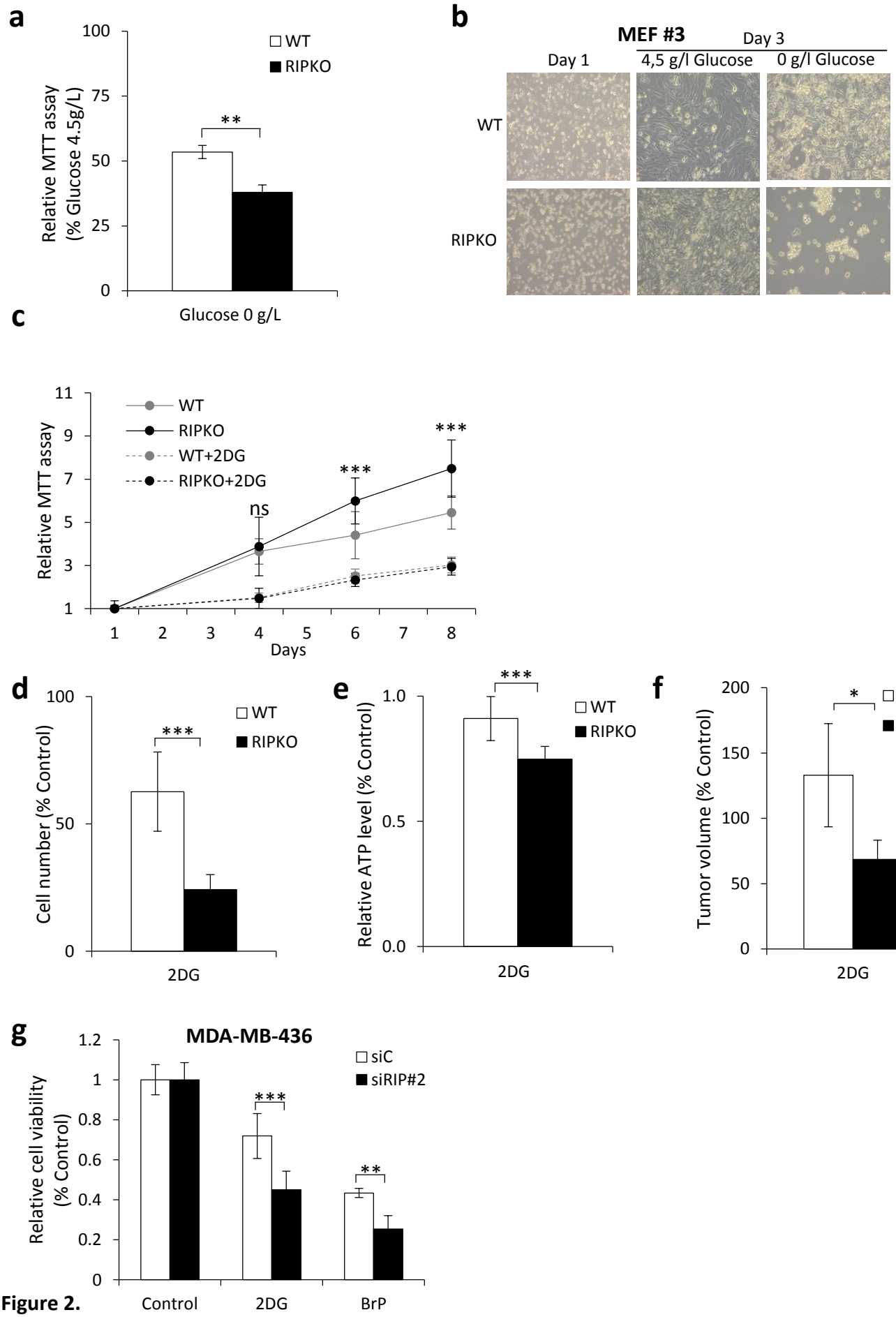
a
Relative MTT assay (% Glucose 4.5g/L)
100
75
50
25
0
WT
RIPKO
**
Glucose 0 g/L
b
MEF #3
Day 3
Day 1
4,5 g/l Glucose
0 g/l Glucose
WT
RIPKO
c
Relative MTT assay
11
9
7
5
3
1
WT
RIPKO
WT+2DG
RIPKO+2DG
ns
***
***
1
2
3
4
5
6
7
8
Days
d
Cell number (% Control)
100
50
0
WT
RIPKO
***
2DG
e
Relative ATP level (% Control)
1.0
0.5
0.0
***
WT
RIPKO
2DG
f
Tumor volume (% Control)
200
150
100
50
0
*
WT
RIPKO
2DG
g
MDA-MB-436
Relative cell viability (% Control)
1.2
1
0.8
0.6
0.4
0.2
0
siC
siRIP#2
***
**
Control
2DG
BrP

Figure 2.

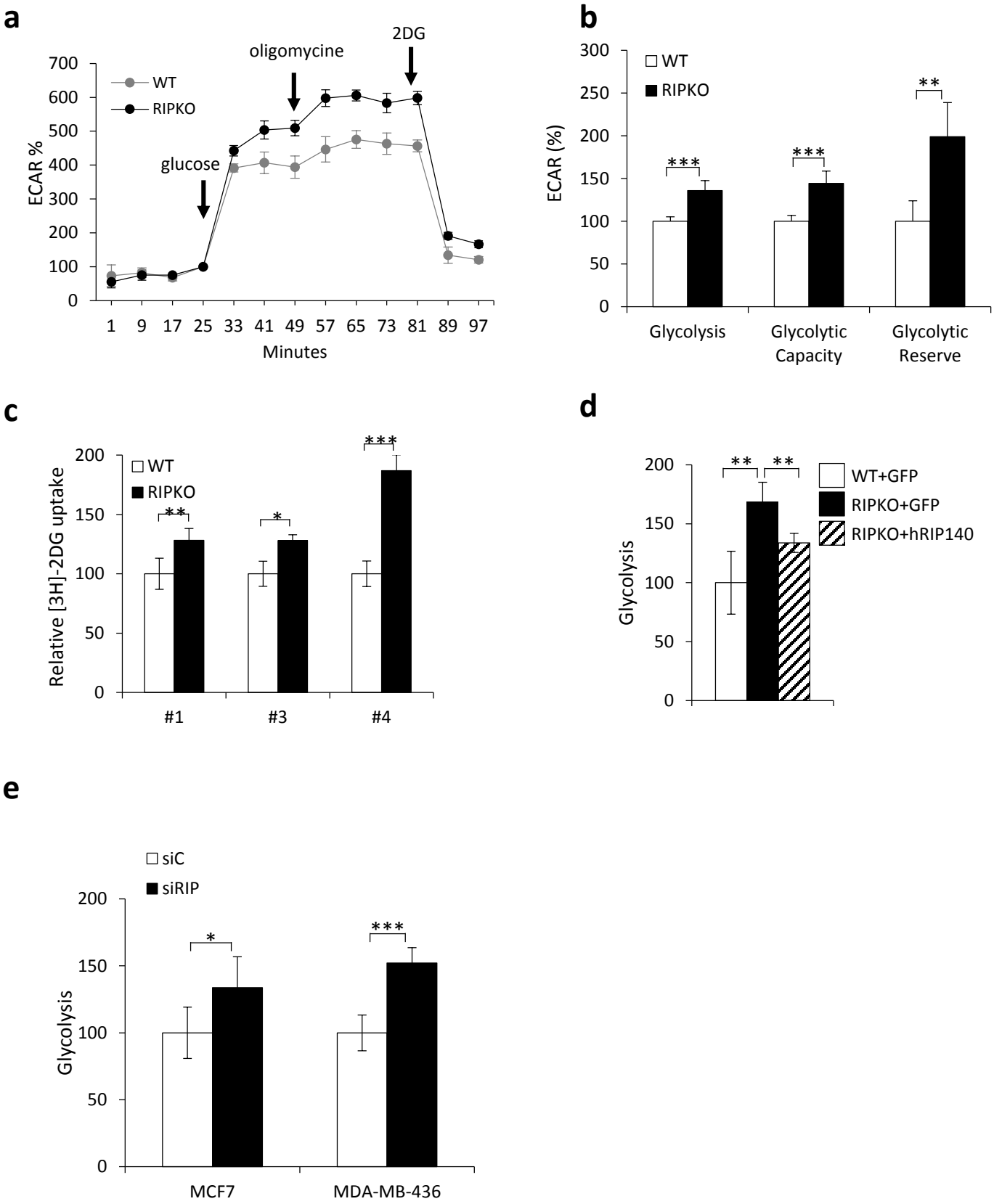
a
ECAR %
700
600
500
400
300
200
100
0
WT
RIPKO
glucose
oligomycine
2DG
1 9 17 25 33 41 49 57 65 73 81 89 97
Minutes
b
ECAR (%)
300
250
200
150
100
50
0
WT
RIPKO
***
***
**
Glycolysis
Glycolytic Capacity
Glycolytic Reserve
c
Relative [3H]-2DG uptake
200
150
100
50
0
WT
RIPKO
**
*
***
#1
#3
#4
d
Glycolysis
200
150
100
50
0
**
**
WT+GFP
RIPKO+GFP
RIPKO+hRIP140
e
siC
siRIP
Glycolysis
200
150
100
50
0
*
***
MCF7
MDA-MB-436

Figure 3.

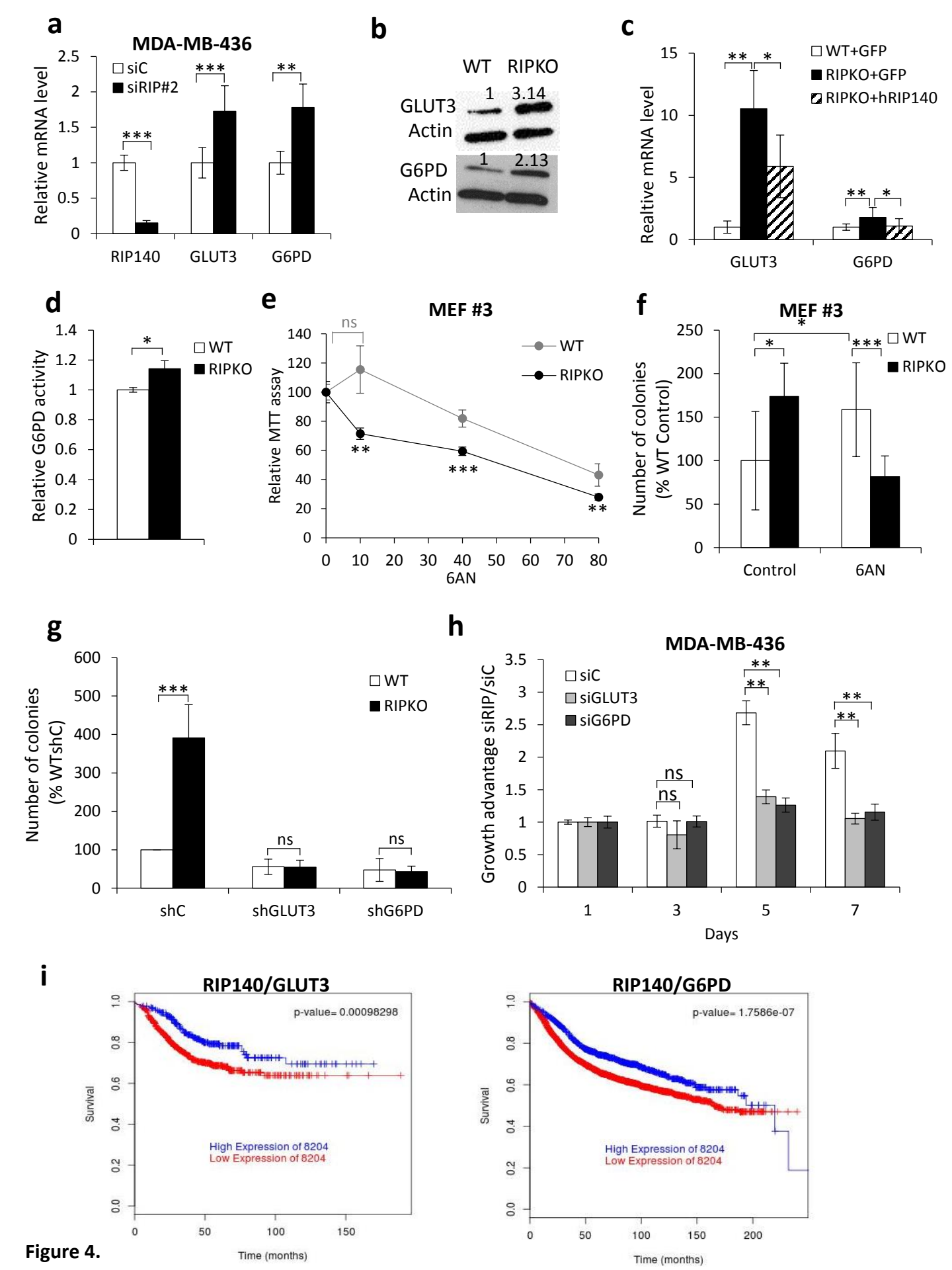
a
MDA-MB-436
siC
siRIP#2
Relative mRNA level
RIP140
GLUT3
G6PD
b
WT
RIPKO
GLUT3
Actin
G6PD
Actin
1
3.14
1
2.13
c
WT+GFP
RIPKO+GFP
RIPKO+hRIP140
Realtive mRNA level
GLUT3
G6PD
d
WT
RIPKO
Relative G6PD activity
e
MEF #3
WT
RIPKO
Relative MTT assay
6AN
ns
f
MEF #3
WT
RIPKO
Number of colonies (% WT Control)
Control
6AN
g
WT
RIPKO
Number of colonies (% WTshC)
shC
shGLUT3
shG6PD
ns
h
MDA-MB-436
siC
siGLUT3
siG6PD
Growth advantage siRIP/siC
Days
ns
i
RIP140/GLUT3
p-value= 0.00098298
High Expression of 8204
Low Expression of 8204
Survival
Time (months)
RIP140/G6PD
p-value= 1.7586e-07
High Expression of 8204
Low Expression of 8204
Survival
Time (months)

Figure 4.

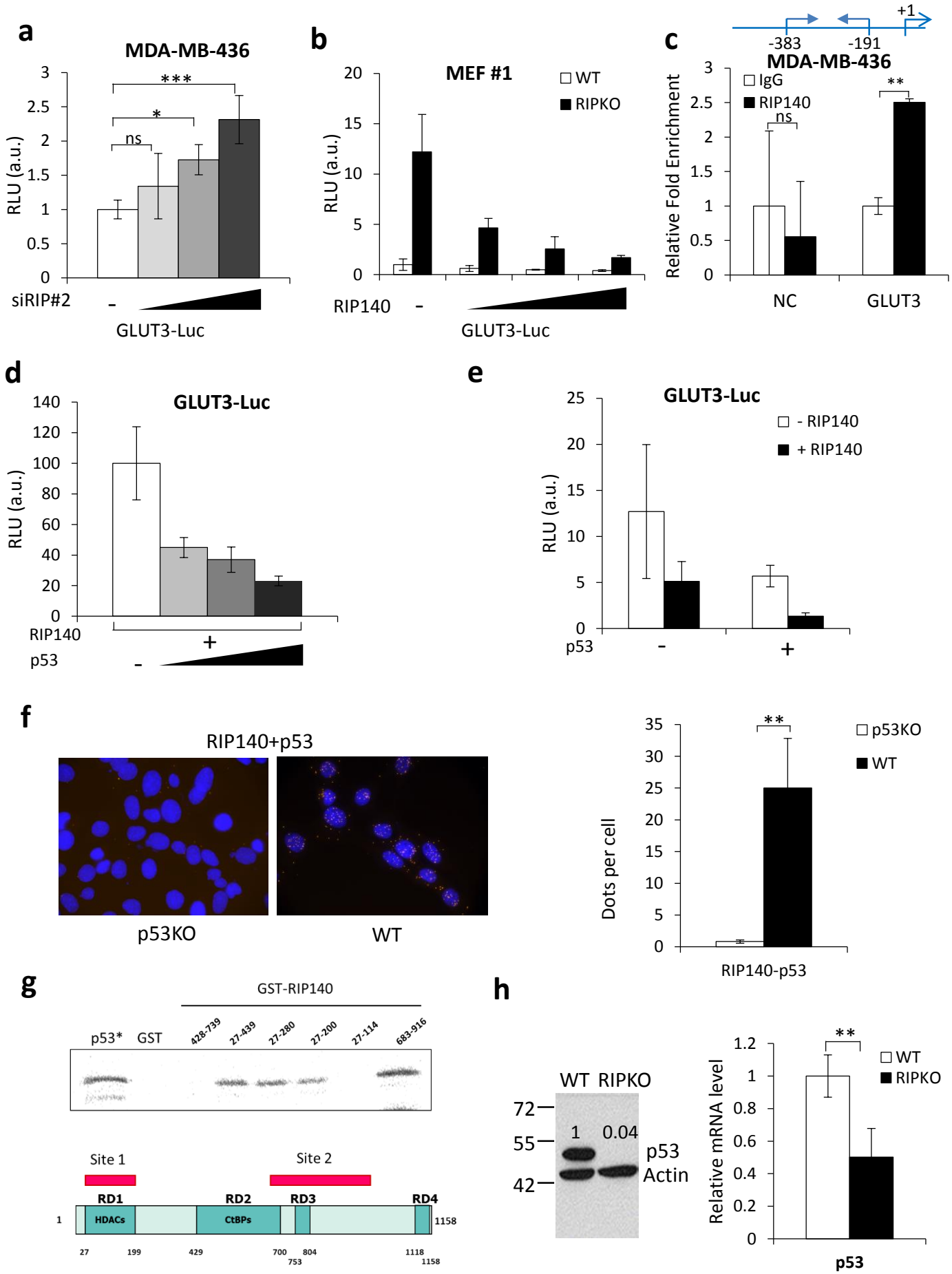
a
MDA-MB-436
RLU (a.u.)
***
*
ns
siRIP#2
-
GLUT3-Luc
b
MEF #1
WT
RIPKO
RLU (a.u.)
RIP140
-
GLUT3-Luc
c
+1
-383
-191
MDA-MB-436
IgG
RIP140
ns
**
Relative Fold Enrichment
NC
GLUT3
d
GLUT3-Luc
RLU (a.u.)
RIP140
+
p53
-
e
GLUT3-Luc
- RIP140
+ RIP140
RLU (a.u.)
p53
-
+
f
RIP140+p53
p53KO
WT
**
p53KO
WT
Dots per cell
RIP140-p53
g
GST-RIP140
p53*
GST
428-739
27-439
27-280
27-200
27-114
683-916
Site 1
Site 2
RD1
RD2
RD3
RD4
HDACs
CtBPs
1
1158
27
199
429
700
804
753
1118
1158
h
WT
RIPKO
72
55
42
1
0.04
p53
Actin
**
WT
RIPKO
Relative mRNA level
p53

Figure 5

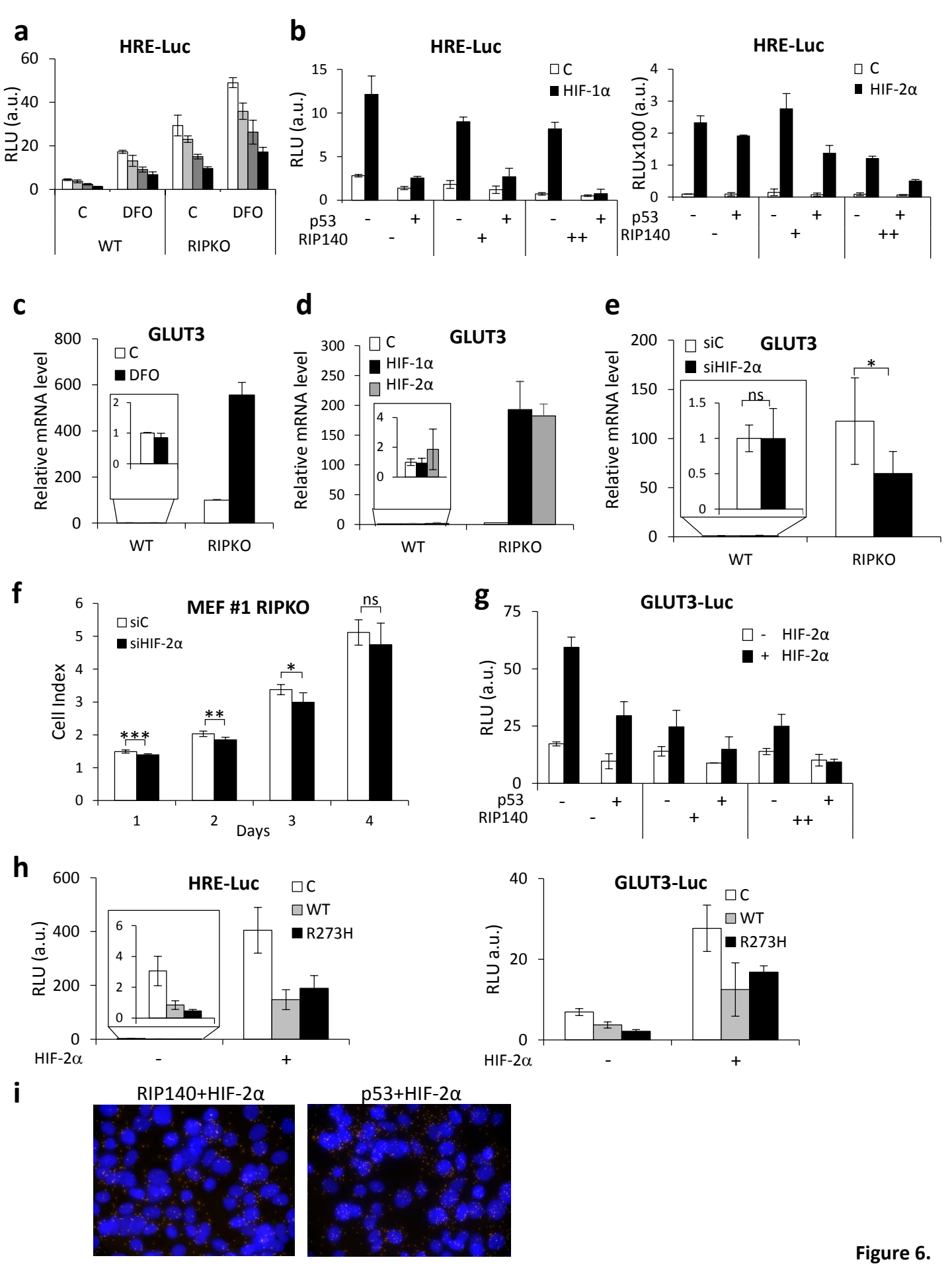
a
HRE-Luc
RLU (a.u.)
60
40
20
0
C
DFO
C
DFO
WT
RIPKO
b
HRE-Luc
RLU (a.u.)
15
10
5
0
C
HIF-1α
p53
RIP140
HRE-Luc
RLUx100 (a.u.)
4
3
2
1
0
C
HIF-2α
p53
RIP140
c
GLUT3
Relative mRNA level
800
600
400
200
0
C
DFO
WT
RIPKO
d
GLUT3
Relative mRNA level
300
250
200
150
100
50
0
C
HIF-1α
HIF-2α
WT
RIPKO
e
GLUT3
Relative mRNA level
200
150
100
50
0
siC
siHIF-2α
ns
*
WT
RIPKO
f
MEF #1 RIPKO
Cell Index
siC
siHIF-2α
***
**
*
ns
Days
g
GLUT3-Luc
RLU (a.u.)
75
50
25
0
- HIF-2α
+ HIF-2α
p53
RIP140
h
HRE-Luc
RLU (a.u.)
600
400
200
0
C
WT
R273H
HIF-2α
GLUT3-Luc
RLU a.u.)
40
20
0
C
WT
R273H
HIF-2α
i
RIP140+HIF-2α
p53+HIF-2α

Figure 6.

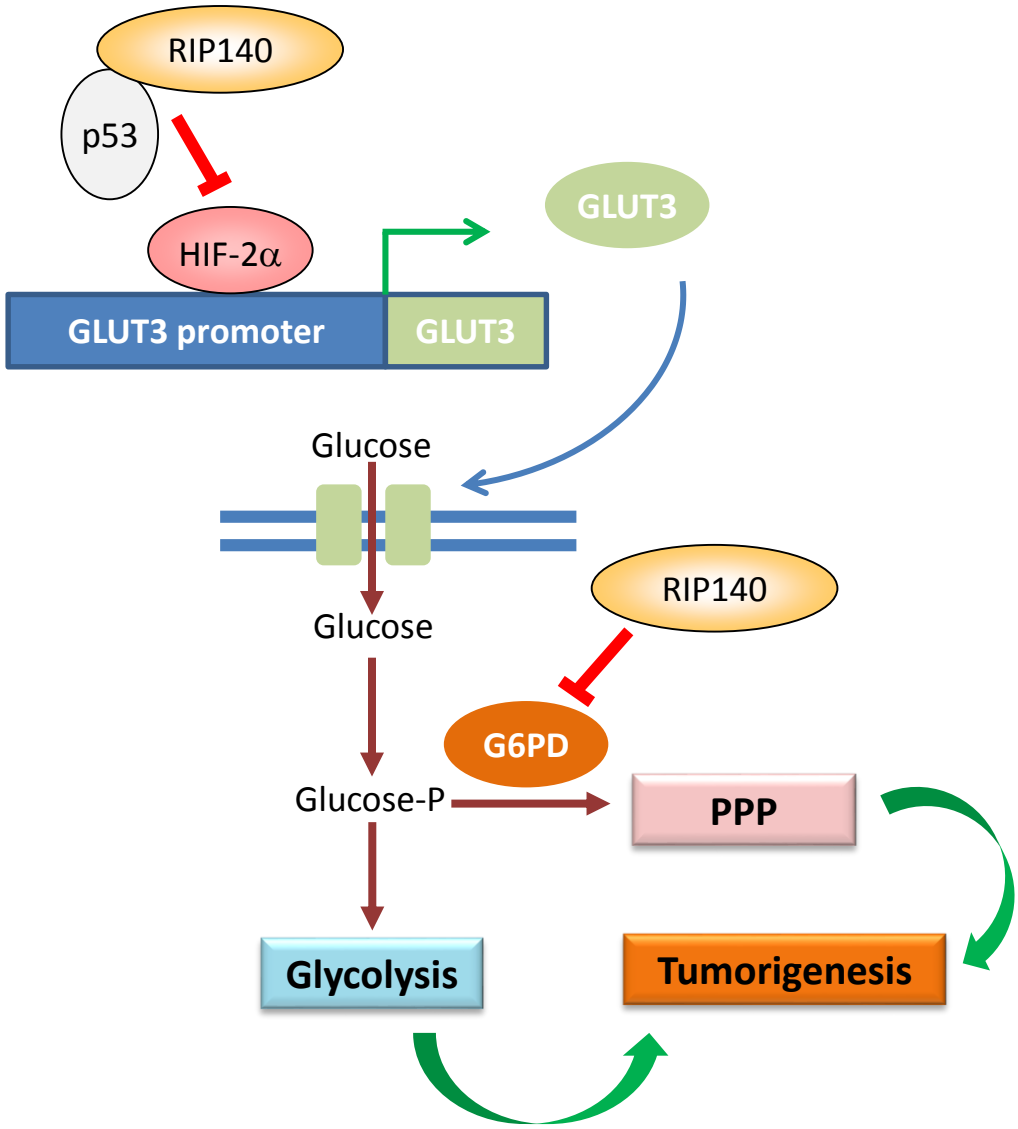
RIP140
p53
HIF-2α
GLUT3
GLUT3 promoter
GLUT3
Glucose
Glucose
RIP140
G6PD
Glucose-P
PPP
Glycolysis
Tumorigenesis

Figure 7.